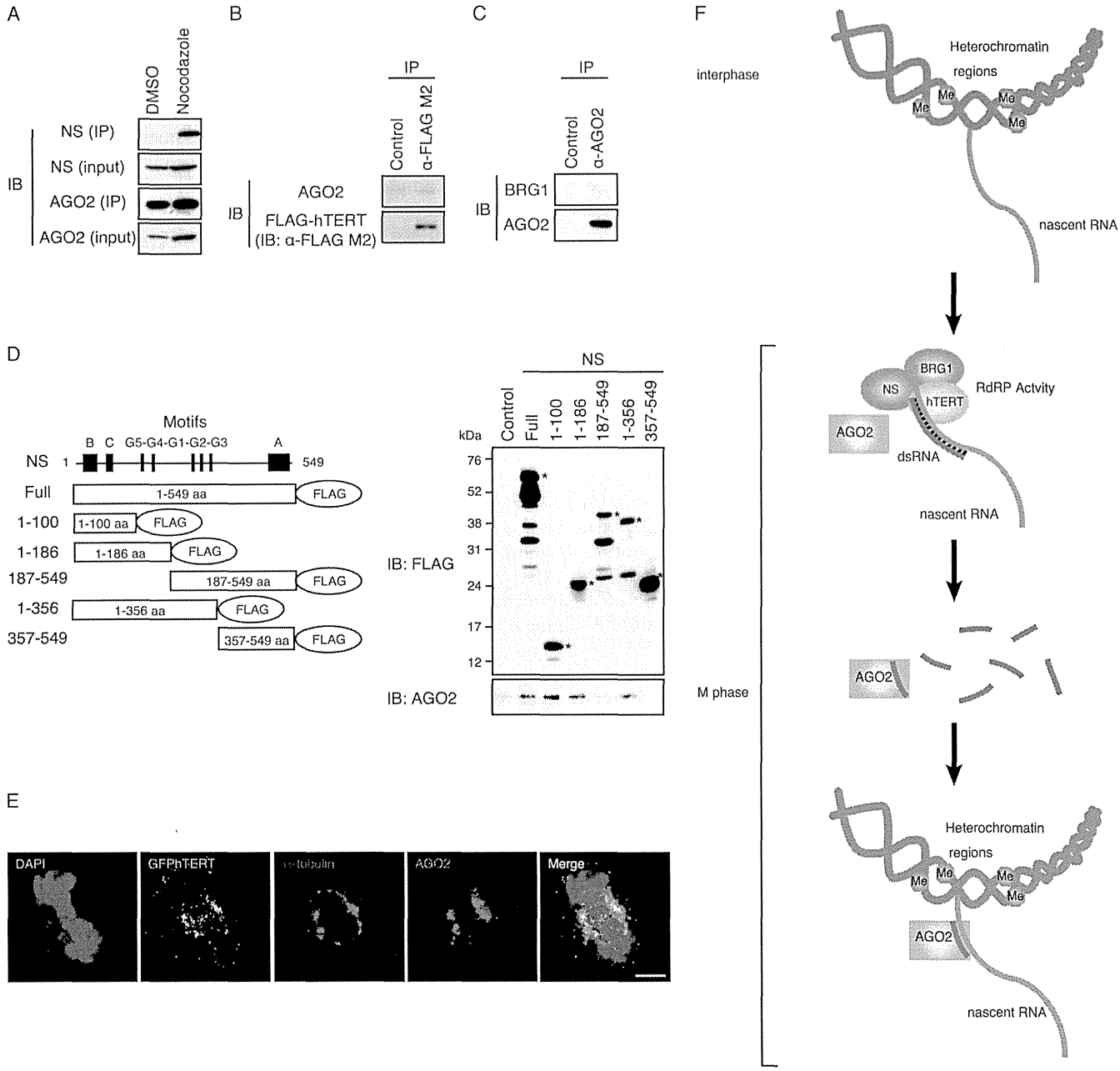

FIG 8 AGO2 is essential for heterochromatin formation. (A) AGO2 interacts with endogenous NS. AGO2 immune complexes were isolated from HeLa cells treated with nocodazole (manipulated) or DMSO (unmanipulated) and immunoblotted with anti-NS and anti-AGO2 antibodies. IB, immunoblot. (B) hTERT does not interact with endogenous AGO2. FLAG-hTERT immune complexes were immunoblotted with anti-AGO2 antibody. (C) BRG1 does not interact with endogenous AGO2. AGO2 immune complexes were immunoblotted with anti-BRG1 antibody. (D) AGO2 interacts with NS. Schematic representation of full-length FLAG epitope-tagged NS and truncation mutants where consensus motifs are represented by boxes. 293T cells were transiently transfected with either an empty vector (Control) or FLAG-tagged NS expression vectors. Immune complexes were isolated using anti-FLAG-M2 antibody and immunoblotted with anti-FLAG M2 and anti-AGO2 antibodies. Asterisks indicate the migration of deletion mutants. Other signals in the upper panel are degradation products. (E) Immunofluorescence of GFP-hTERT, α-tubulin, and AGO2. HeLa-GFP-hTERT cells were immunostained with antibodies against α-tubulin and AGO2 followed by DAPI staining. Mitotic cells are shown. Scale bar, 5 μm. (F) A model for hTERT-mediated heterochromatin regulation in repetitive chromosomal regions. A nascent RNA transcribed from heterochromatic regions in cycling cells interacts with the TBN complex in mitosis. Antisense RNAs synthesized by the RdRP activity of hTERT are targeted to the heterochromatic regions to suppress the expression in mitosis.

and the Cajal bodies during assembly and associates with telomeres during S phase while forming *hTERC*-independent complexes with BRG1 and NS during mitosis.

TBN and RdRP activity. In *S. pombe*, RdRP localizes to centromeres and maintains heterochromatin at the centromere. Inhibition of RdRP activity leads to loss of siRNAs that are associated with the RITS complex and correlates with loss of transcriptional silencing and heterochromatin at centromeres (3). In addition,

when RdRP activity is inhibited, siRNAs that are usually associated with the RITS complex are lost (4). In *C. elegans*, the RdRP localizes to chromosomes and is required for proper chromosome segregation (5, 6). In both *S. pombe* and *C. elegans*, the RNAi pathway is crucial for heterochromatin assembly at centromeres and is required for the accurate segregation of chromosomes during mitosis.

The *S. pombe* RDRC contains the RdRP Rdp1 and the RNA helicase Hrr1 (2). BRG1 has helicase (43) and ATPase (44) activity and is a component of the SNF/SWI chromatin remodeling complex (11). NS is a GTPase and is essential in pre-rRNA processing (45). In addition, we found that AGO2 interacts with NS and is required for the regulation of *hLINE1* and *alphoid* expression. Since hTERT also exhibits RdRP activity separate from its function as telomerase (10), these observations suggest that the TBN complex contains proteins with similar functions to those found in the RdRP complexes involved in the regulation of heterochromatin in *S. pombe* and *C. elegans*.

Prior attempts to identify mammalian RdRPs based on homology to RdRP components in other organisms failed to identify homologous proteins. However, recent work suggests that proteins that are not direct homologs may serve similar functions in different organisms. For example, RNA polymerase II has been predicted to exhibit RdRP activity (46). These observations suggest that the TBN complex may function in a manner analogous to the RDRC/RITS complex in *S. pombe*.

Moreover, we found that AGO2 is involved in heterochromatin maintenance through its interaction with the TBN complex (Fig. 8A and D). In contrast, DICER1 is dispensable for the heterochromatin maintenance mediated by TBN-RdRP activity. Since Dicer-independent secondary siRNAs generated by RdRP in a *de novo* pathway have been reported in *C. elegans* (21, 47, 48), we speculate that the TBN complex maintains heterochromatin during mitosis using *de novo*-synthesized short RNAs in an AGO2-dependent but a DICER1-independent manner. Since prior reports showed that deletion of Dicer affects the maintenance of heterochromatin in human and murine cells (49, 50), other siRNA-dependent mechanisms may also regulate heterochromatin separate from hTERT.

In consonance with these observations, we found that suppression of components of the TBN complex affects the status of heterochromatin at *alphoid* and *hLINE1* elements. Specifically, we found that hTERT binds to ssRNA transcribed from these regions and produces dsRNAs that are processed into siRNAs. Similar to what has been observed in yeast and worms, these siRNAs play a key role in regulating the status of heterochromatin in these regions. To confirm that the TBN complex is essential for the regulation of heterochromatin in these regions, we confirmed that deletion of TERT also affects the expression of RNAs transcribed from *IAP*, *mLINE1 Type A*, and *mLINE1 Type Tf* (Fig. 4E and F) and used the telomerase inhibitor β-rubromycin to inhibit hTERT. Together, these genetic and pharmacologic observations support the notion that hTERT has functional roles at nontelomeric regions, which are essential for heterochromatin formation. We note that suppression of NS failed to affect the transcription of *alphoid* repeats (Fig. 7K). NS is closely related to GNL3L, which has been reported to have redundant functions with NS (15, 51). Indeed, we have confirmed that GNL3L physically interacts with hTERT and BRG1 and forms a complex that maintains tumor initiating cells (15).

Prior work has demonstrated that the maintenance of centromeric heterochromatin is necessary for proper chromosomal segregation during mitotic progression in both *S. pombe* (28) and human cells (29), and regulation of expression of *alphoid* transcripts is required for mitosis (49). Since both centromeric *alphoid* regions and transposable elements are maintained in a heterochromatic state during mitosis (Fig. 3 and 4), we speculate that the regulation of heterochromatin at *alphoid* regions and/or *hLINE1* is directly connected to proper progression of mitosis. Moreover, since these repetitive elements have been implicated in centromere maintenance (49, 52), disrupting these functions may promote genomic instability (53). Indeed, prior work suggested that TERT promotes genome stability by providing capping functions, only some of which involve the maintenance of telomeres (8, 13).

Taking these result together, we propose a model for heterochromatin regulation through the RNAi pathway mediated by the TBN complex (Fig. 8F). Specifically, the TBN complex is upregulated in M phase and binds to nascent RNA from *alphoid* and *hLINE1* transcripts. These RNAs serve as templates for dsRNA synthesis by hTERT-RdRP and are further processed in an AGO2-dependent manner to produce siRNAs that regulate the state of heterochromatin at these loci.

Epigenetic modifications link the TBN complex with tumors or TICs. TERT, BRG1, and NS are upregulated in malignant cells (40, 54, 55). Thus, the upregulation of TERT, BRG1, or NS may lead to aberrant heterochromatin formation due to the enhanced RdRP activity. We speculate that defective heterochromatin caused by enhanced RdRP activity may also contribute to tumor initiation and/or progression. Moreover, the TBN complex maintains the functions of tumor initiating cells (TICs) (15). These observations suggest that inhibiting these various hTERT functions may prove useful in sensitizing cancer stem cells to cytotoxic therapies such as radiation and chemotherapy.

ACKNOWLEDGMENTS

We thank Fuyuki Ishikawa for the gift of mTERT-knockout mice and Satomi Kuramochi-Miyagawa, Tokio Tani, and Hiroyuki Seimiya for providing technical assistance with RT-PCR analysis of LINE elements, satellite I RT-PCR, and TRAP assays, respectively. We thank Medical and Biological Laboratories Co., Ltd., for their assistance in creating the hTERT MAb.

This work was supported in part by a Grant-in-Aid for Young Scientists (B) (S.O.), a funding program for the Next Generation World-Leading Researchers (NEXT program) (K.M.), the Takeda Science Foundation (K.M.), the Kato Memorials Bioscience Foundation (K.M.), and National Cancer Center Research and Development Funds (23-A-8 to T.S., 23-A-7 to K.K., and 23-B-5 to K.M.). N.O. was a Research Fellow of the Japan Society for the Promotion of Science.

N.O., M.Y., S.O., K.K., Y.M., S.Y., T.K.I., T.M., and H.N. performed experiments. Y.T. and T.S. designed and carried out the bioinformatics analyses. M.Y., Y.M., and K.M. designed the experiments and discussed the interpretation of the results. K.M. and Y.M. wrote the manuscript.

REFERENCES

1. **Verdel A, Jia S, Gerber S, Sugiyama T, Gygi S, Grewal SI, Moazed D.** 2004. RNAi-mediated targeting of heterochromatin by the RITS complex. Science 303:672–676. http://dx.doi.org/10.1126/science.1093686.
2. **Motamedi MR, Verdel A, Colmenares SU, Gerber SA, Gygi SP, Moazed D.** 2004. Two RNAi complexes, RITS and RDRC, physically interact and localize to noncoding centromeric RNAs. Cell 119:789–802. http://dx.doi.org/10.1016/j.cell.2004.11.034.
3. **Sugiyama T, Cam H, Verdel A, Moazed D, Grewal SI.** 2005. RNA-

dependent RNA polymerase is an essential component of a self-enforcing loop coupling heterochromatin assembly to siRNA production. Proc. Natl. Acad. Sci. U. S. A. 102:152–157. http://dx.doi.org/10.1073/pnas.0407641102.
4. Wassenegger M. 2005. The role of the RNAi machinery in heterochromatin formation. Cell 122:13–16. http://dx.doi.org/10.1016/j.cell.2005.06.034.
5. Claycomb JM, Batista PJ, Pang KM, Gu W, Vasale JJ, van Wolfswinkel JC, Chaves DA, Shirayama M, Mitani S, Ketting RF, Conte D, Jr, Mello CC. 2009. The Argonaute CSR-1 and its 22G-RNA cofactors are required for holocentric chromosome segregation. Cell 139:123–134. http://dx.doi.org/10.1016/j.cell.2009.09.014.
6. van Wolfswinkel JC, Claycomb JM, Batista PJ, Mello CC, Berezikov E, Ketting RF. 2009. CDE-1 affects chromosome segregation through uridylation of CSR-1-bound siRNAs. Cell 139:135–148. http://dx.doi.org/10.1016/j.cell.2009.09.012.
7. Castel SE, Martienssen RA. 2013. RNA interference in the nucleus: roles for small RNAs in transcription, epigenetics and beyond. Nat. Rev. Genet. 14:100–112. http://dx.doi.org/10.1038/nrg3355.
8. Masutomi K, Possemato R, Wong JM, Currier JL, Tothova Z, Manola JB, Ganesan S, Lansdorp PM, Collins K, Hahn WC. 2005. The telomerase reverse transcriptase regulates chromatin state and DNA damage responses. Proc. Natl. Acad. Sci. U. S. A. 102:8222–8227. http://dx.doi.org/10.1073/pnas.0503095102.
9. Sarin KY, Cheung P, Gilison D, Lee E, Tennen RI, Wang E, Artandi MK, Oro AE, Artandi SE. 2005. Conditional telomerase induction causes proliferation of hair follicle stem cells. Nature 436:1048–1052. http://dx.doi.org/10.1038/nature03836.
10. Maida Y, Yasukawa M, Furuuchi M, Lassmann T, Possemato R, Okamoto N, Kasim V, Hayashizaki Y, Hahn WC, Masutomi K. 2009. An RNA-dependent RNA polymerase formed by TERT and the RMRP RNA. Nature 461:230–235. http://dx.doi.org/10.1038/nature08283.
11. Park JI, Venteicher AS, Hong JY, Choi J, Jun S, Shkreli M, Chang W, Meng Z, Cheung P, Ji H, McLaughlin M, Veenstra TD, Nusse R, McCrea PD, Artandi SE. 2009. Telomerase modulates Wnt signalling by association with target gene chromatin. Nature 460:66–72. http://dx.doi.org/10.1038/nature08137.
12. Stewart SA, Hahn WC, O'Connor BF, Banner EN, Lundberg AS, Modha P, Mizuno H, Brooks MW, Fleming M, Zimonjic DB, Popescu NC, Weinberg RA. 2002. Telomerase contributes to tumorigenesis by a telomere length-independent mechanism. Proc. Natl. Acad. Sci. U. S. A. 99:12606–12611. http://dx.doi.org/10.1073/pnas.182407599.
13. Zhu J, Wang H, Bishop JM, Blackburn EH. 1999. Telomerase extends the lifespan of virus-transformed human cells without net telomere lengthening. Proc. Natl. Acad. Sci. U. S. A. 96:3723–3728. http://dx.doi.org/10.1073/pnas.96.7.3723.
14. Venteicher AS, Abreu EB, Meng Z, McCann KE, Terns RM, Veenstra TD, Terns MP, Artandi SE. 2009. A human telomerase holoenzyme protein required for Cajal body localization and telomere synthesis. Science 323:644–648. http://dx.doi.org/10.1126/science.1165357.
15. Okamoto N, Yasukawa M, Nguyen C, Kasim V, Maida Y, Possemato R, Shibata T, Ligon KL, Fukami K, Hahn WC, Masutomi K. 2011. Maintenance of tumor initiating cells of defined genetic composition by nucleostemin. Proc. Natl. Acad. Sci. U. S. A. 108:20388–20393. http://dx.doi.org/10.1073/pnas.1015171108.
16. Kuhara M, Yoshino T, Shiokawa M, Okabe T, Mizoguchi S, Yabuhara A, Takeyama H, Matsunaga T. 2009. Magnetic separation of human podocalyxin-like protein 1 (hPCLP1)-positive cells from peripheral blood and umbilical cord blood using anti-hPCLP1 monoclonal antibody and protein A expressed on bacterial magnetic particles. Cell Struct. Funct. 34:23–30. http://dx.doi.org/10.1247/csf.08043.
17. Hahn WC, Counter CM, Lundberg AS, Beijersbergen RL, Brooks MW, Weinberg RA. 1999. Creation of human tumour cells with defined genetic elements. Nature 400:464–468. http://dx.doi.org/10.1038/22780.
18. Summers MK, Bothos J, Halazonetis TD. 2005. The CHFR mitotic checkpoint protein delays cell cycle progression by excluding Cyclin B1 from the nucleus. Oncogene 24:2589–2598. http://dx.doi.org/10.1038/sj.onc.1208428.
19. Hirashima K, Migita T, Sato S, Muramatsu Y, Ishikawa Y, Seimiya H. 2013. Telomere length influences cancer cell differentiation *in vivo*. Mol. Cell. Biol. 33:2988–2995. http://dx.doi.org/10.1128/MCB.00136-13.
20. Thibault MM, Buschmann MD. 2006. Migration of bone marrow stromal cells in 3D: 4 color methodology reveals spatially and temporally coordinated events. Cell Motil. Cytoskeleton 63:725–740. http://dx.doi.org/10.1002/cm.20160.
21. Aoki K, Moriguchi H, Yoshioka T, Okawa K, Tabara H. 2007. In vitro analyses of the production and activity of secondary small interfering RNAs in *C. elegans*. EMBO J. 26:5007–5019. http://dx.doi.org/10.1038/sj.emboj.7601910.
22. Masutomi K, Yu EY, Khurts S, Ben-Porath I, Currier JL, Metz GB, Brooks MW, Kaneko S, Murakami S, DeCaprio JA, Weinberg RA, Stewart SA, Hahn WC. 2003. Telomerase maintains telomere structure in normal human cells. Cell 114:241–253. http://dx.doi.org/10.1016/S0092-8674(03)00550-6.
23. Zhu XD, Kuster B, Mann M, Petrini JH, de Lange T. 2000. Cell-cycle-regulated association of RAD50/MRE11/NBS1 with TRF2 and human telomeres. Nat. Genet. 25:347–352. http://dx.doi.org/10.1038/77139.
24. Wu P, van Overbeek M, Rooney S, de Lange T. 2010. Apollo contributes to G overhang maintenance and protects leading-end telomeres. Mol. Cell 39:606–617. http://dx.doi.org/10.1016/j.molcel.2010.06.031.
25. Takai KK, Kibe T, Donigian JR, Frescas D, de Lange T. 2011. Telomere protection by TPP1/POT1 requires tethering to TIN2. Mol. Cell 44:647–659. http://dx.doi.org/10.1016/j.molcel.2011.08.043.
26. Hirai Y, Masutomi K, Ishikawa F. 2012. Kinetics of DNA replication and telomerase reaction at a single-seeded telomere in human cells. Genes Cells 17:186–204. http://dx.doi.org/10.1111/j.1365-2443.2012.01581.x.
27. Nishiyama A, Muraki K, Saito M, Ohsumi K, Kishimoto T, Ishikawa F. 2006. Cell-cycle-dependent *Xenopus* TRF1 recruitment to telomere chromatin regulated by Polo-like kinase. EMBO J. 25:575–584. http://dx.doi.org/10.1038/sj.emboj.7600964.
28. Dubey RN, Nakwal N, Bisht KK, Saini A, Haldar S, Singh J. 2009. Interaction of APC/C-E3 ligase with Swi6/HP1 and Clr4/Suv39 in heterochromatin assembly in fission yeast. J. Biol. Chem. 284:7165–7176. http://dx.doi.org/10.1074/jbc.M806461200.
29. Heit R, Rattner JB, Chan GK, Hendzel MJ. 2009. G_2 histone methylation is required for the proper segregation of chromosomes. J. Cell Sci. 122:2957–2968. http://dx.doi.org/10.1242/jcs.045351.
30. Mitchell AR, Gosden JR, Miller DA. 1985. A cloned sequence, p82H, of the alphoid repeated DNA family found at the centromeres of all human chromosomes. Chromosoma 92:369–377. http://dx.doi.org/10.1007/BF00327469.
31. Yu F, Zingler N, Schumann G, Stratling WH. 2001. Methyl-CpG-binding protein 2 represses LINE-1 expression and retrotransposition but not Alu transcription. Nucleic Acids Res. 29:4493–4501. http://dx.doi.org/10.1093/nar/29.21.4493.
32. Peters AH, Kubicek S, Mechtler K, O'Sullivan RJ, Derijck AA, Perez-Burgos L, Kohlmaier A, Opravil S, Tachibana M, Shinkai Y, Martens JH, Jenuwein T. 2003. Partitioning and plasticity of repressive histone methylation states in mammalian chromatin. Mol. Cell 12:1577–1589. http://dx.doi.org/10.1016/S1097-2765(03)00477-5.
33. Ghoshal K, Datta J, Majumder S, Bai S, Dong X, Parthun M, Jacob ST. 2002. Inhibitors of histone deacetylase and DNA methyltransferase synergistically activate the methylated metallothionein I promoter by activating the transcription factor MTF-1 and forming an open chromatin structure. Mol. Cell. Biol. 22:8302–8319. http://dx.doi.org/10.1128/MCB.22.23.8302-8319.2002.
34. Heidmann O, Heidmann T. 1991. Retrotransposition of a mouse IAP sequence tagged with an indicator gene. Cell 64:159–170. http://dx.doi.org/10.1016/0092-8674(91)90217-M.
35. Kuramochi-Miyagawa S, Watanabe T, Gotoh K, Totoki Y, Toyoda A, Ikawa M, Asada N, Kojima K, Yamaguchi Y, Ijiri TW, Hata K, Li E, Matsuda Y, Kimura T, Okabe M, Sakaki Y, Sasaki H, Nakano T. 2008. DNA methylation of retrotransposon genes is regulated by Piwi family members MILI and MIWI2 in murine fetal testes. Genes Dev. 22:908–917. http://dx.doi.org/10.1101/gad.1640708.
36. Ueno T, Takahashi H, Oda M, Mizunuma M, Yokoyama A, Goto Y, Mizushina Y, Sakaguchi K, Hayashi H. 2000. Inhibition of human telomerase by rubromycins: implication of spiroketal system of the compounds as an active moiety. Biochemistry 39:5995–6002. http://dx.doi.org/10.1021/bi992661i.
37. Lue NF, Bosoy D, Moriarty TJ, Autexier C, Altman B, Leng S. 2005. Telomerase can act as a template- and RNA-independent terminal transferase. Proc. Natl. Acad. Sci. U. S. A. 102:9778–9783. http://dx.doi.org/10.1073/pnas.0502252102.
38. Volpe TA, Kidner C, Hall IM, Teng G, Grewal SI, Martienssen RA. 2002. Regulation of heterochromatic silencing and histone H3 lysine-9

methylation by RNAi. Science 297:1833–1837. http://dx.doi.org/10.1126/science.1074973.
39. Alessio N, Squillaro T, Cipollaro M, Bagella L, Giordano A, Galderisi U. 2010. The BRG1 ATPase of chromatin remodeling complexes is involved in modulation of mesenchymal stem cell senescence through RB-P53 pathways. Oncogene 29:5452–5463. http://dx.doi.org/10.1038/onc.2010.285.
40. Tsai RY, McKay RD. 2002. A nucleolar mechanism controlling cell proliferation in stem cells and cancer cells. Genes Dev. 16:2991–3003. http://dx.doi.org/10.1101/gad.55671.
41. Listerman I, Gazzaniga FS, Blackburn EH. 2014. An investigation of the effects of the core protein telomerase reverse transcriptase on wnt signaling in breast cancer cells. Mol. Cell. Biol. 34:280–289. http://dx.doi.org/10.1128/MCB.00844-13.
42. Wong JM, Kusdra L, Collins K. 2002. Subnuclear shuttling of human telomerase induced by transformation and DNA damage. Nat. Cell Biol. 4:731–736. http://dx.doi.org/10.1038/ncb846.
43. Muchardt C, Yaniv M. 1999. ATP-dependent chromatin remodelling: SWI/SNF and Co. are on the job. J. Mol. Biol. 293:187–198. http://dx.doi.org/10.1006/jmbi.1999.2999.
44. Khavari PA, Peterson CL, Tamkun JW, Mendel DB, Crabtree GR. 1993. BRG1 contains a conserved domain of the SWI2/SNF2 family necessary for normal mitotic growth and transcription. Nature 366:170–174. http://dx.doi.org/10.1038/366170a0.
45. Romanova L, Grand A, Zhang L, Rayner S, Katoku-Kikyo N, Kellner S, Kikyo N. 2009. Critical role of nucleostemin in pre-rRNA processing. J. Biol. Chem. 284:4968–4977. http://dx.doi.org/10.1074/jbc.M804594200.
46. Lehmann E, Brueckner F, Cramer P. 2007. Molecular basis of RNA-dependent RNA polymerase II activity. Nature 450:445–449. http://dx.doi.org/10.1038/nature06290.
47. Sijen T, Steiner FA, Thijssen KL, Plasterk RH. 2007. Secondary siRNAs result from unprimed RNA synthesis and form a distinct class. Science 315:244–247. http://dx.doi.org/10.1126/science.1136699.
48. Pak J, Fire A. 2007. Distinct populations of primary and secondary effectors during RNAi in *C. elegans*. Science 315:241–244. http://dx.doi.org/10.1126/science.1132839.
49. Fukagawa T, Nogami M, Yoshikawa M, Ikeno M, Okazaki T, Takami Y, Nakayama T, Oshimura M. 2004. Dicer is essential for formation of the heterochromatin structure in vertebrate cells. Nat. Cell Biol. 6:784–791. http://dx.doi.org/10.1038/ncb1155.
50. Kanellopoulou C, Muljo SA, Kung AL, Ganesan S, Drapkin R, Jenuwein T, Livingston DM, Rajewsky K. 2005. Dicer-deficient mouse embryonic stem cells are defective in differentiation and centromeric silencing. Genes Dev. 19:489–501. http://dx.doi.org/10.1101/gad.1248505.
51. Meng L, Hsu JK, Tsai RY. 2011. GNL3L depletion destabilizes MDM2 and induces p53-dependent G_2/M arrest. Oncogene 30:1716–1726. http://dx.doi.org/10.1038/onc.2010.550.
52. Chueh AC, Northrop EL, Brettingham-Moore KH, Choo KH, Wong LH. 2009. LINE retrotransposon RNA is an essential structural and functional epigenetic component of a core neocentromeric chromatin. PLoS Genet. 5:e1000354. http://dx.doi.org/10.1371/journal.pgen.1000354.
53. Symer DE, Connelly C, Szak ST, Caputo EM, Cost GJ, Parmigiani G, Boeke JD. 2002. Human l1 retrotransposition is associated with genetic instability in vivo. Cell 110:327–338. http://dx.doi.org/10.1016/S0092-8674(02)00839-5.
54. Shay JW, Wright WE. 2001. Telomeres and telomerase: implications for cancer and aging. Radiat. Res. 155:188–193. http://dx.doi.org/10.1667/0033-7587(2001)155[0188:TATIFC]2.0.CO;2.
55. Sentani K, Oue N, Kondo H, Kuraoka K, Motoshita J, Ito R, Yokozaki H, Yasui W. 2001. Increased expression but not genetic alteration of BRG1, a component of the SWI/SNF complex, is associated with the advanced stage of human gastric carcinomas. Pathobiology 69:315–320. http://dx.doi.org/10.1159/000064638.
56. Murray V, Monchawin C. 1994. A polymerase chain reaction on human alphoid DNA produces a characteristic ladder of bands. Biochem. Mol. Biol. Int. 34:323–327.

J Gastroenterol
DOI 10.1007/s00535-014-1007-2

The Japanese Society of Gastroenterology

ORIGINAL ARTICLE—LIVER, PANCREAS, AND BILIARY TRACT

Association between *Wisteria floribunda* agglutinin-positive Mac-2 binding protein and the fibrosis stage of non-alcoholic fatty liver disease

Masanori Abe · Teruki Miyake · Atsushi Kuno · Yasuharu Imai · Yoshiyuki Sawai · Keisuke Hino · Yuichi Hara · Shuhei Hige · Michiie Sakamoto · Gotaro Yamada · Masayoshi Kage · Masaaki Korenaga · Yoichi Hiasa · Masashi Mizokami · Hisashi Narimatsu

Received: 12 September 2014 / Accepted: 8 October 2014

Abstract
Background Accurately evaluating liver fibrosis in patients with non-alcoholic fatty liver disease (NAFLD) is important for identifying those who may develop complications. The aims of this study were (1) to measure serum *Wisteria floribunda* agglutinin-positive Mac-2 binding protein (WFA$^+$-M2BP) using the glycan sugar chain-based immunoassay and (2) to compare the results with clinical assessments of fibrosis.
Methods Serum WFA$^+$-M2BP values were retrospectively evaluated in 289 patients with NAFLD who had undergone liver biopsy. Histological findings were evaluated by three blinded, experienced liver-specific pathologists.
Results For stages 0 ($n = 35$), 1 ($n = 113$), 2 ($n = 49$), 3 ($n = 41$), and 4 ($n = 51$) of liver fibrosis, the serum WFA$^+$-M2BP cutoff indexes were 0.57, 0.70, 1.02, 1.57, and 2.96, respectively. Multivariate regression analysis showed that serum WFA$^+$-M2BP values were associated with the stage of fibrosis (≥stage 2). The areas under the receiver operating characteristic curve (AUROC), sensitivity, and specificity of serum WFA$^+$-M2BP were 0.876, 85.9, and 74.6 %, respectively, for severe fibrosis (≥stage 3) and were 0.879, 74.6, and 87.0 %, respectively, for cirrhosis. When compared with six non-invasive conven-

Electronic supplementary material The online version of this article (doi:10.1007/s00535-014-1007-2) contains supplementary material, which is available to authorized users.

M. Abe (✉) · T. Miyake · Y. Hiasa
Department of Gastroenterology and Metabology, Ehime University Graduate School of Medicine, Toon, Ehime 791-0295, Japan
e-mail: masaben@m.ehime-u.ac.jp

M. Abe · T. Miyake · A. Kuno · Y. Imai · Y. Sawai · K. Hino · Y. Hara · S. Hige · M. Sakamoto · M. Korenaga · M. Mizokami · H. Narimatsu
The Hepatitis Glyco-biomarker Study Group, Tokyo, Japan

A. Kuno · H. Narimatsu
Research Center for Medical Glycoscience, National Institute of Advanced Industrial Science and Technology, Tsukuba, Ibaraki, Japan

Y. Imai · Y. Sawai
Department of Gastroenterology, Ikeda Municipal Hospital, Ikeda, Osaka, Japan

K. Hino · Y. Hara
Department of Hepatology and Pancreatology, Kawasaki Medical School, Kurashiki, Okayama, Japan

S. Hige
Department of Hepatology, Sapporo-Kosei General Hospital, Sapporo, Hokkaido, Japan

M. Sakamoto
Department of Pathology, Keio University School of Medicine, Tokyo, Japan

G. Yamada
Department of General Internal Medicine 2, Kawasaki Medical School, Kurashiki, Okayama, Japan

M. Kage
Department of Diagnostic Pathology, Kurume University Hospital, Kurume, Fukuoka, Japan

M. Korenaga · M. Mizokami
The Research Center for Hepatitis and Immunology, National Center for Global Health and Medicine, Ichikawa, Chiba, Japan

Published online: 18 October 2014

tional markers, serum WFA^+-M2BP had the greatest AUROC for diagnosing severe fibrosis and cirrhosis.
Conclusions Serum WFA^+-M2BP values are useful for assessing the stage of liver fibrosis in patients with NAFLD.

Keywords Mac-2 binding protein · Glycoprotein · Non-alcoholic fatty liver disease · Fibrosis marker · Cirrhosis

Introduction

Non-alcoholic fatty liver disease (NAFLD) is one of the most common liver diseases worldwide and is recognized as the hepatic manifestation of metabolic syndrome [1–3]. NAFLD can be classified as simple steatosis or non-alcoholic steatohepatitis (NASH), a progressive form of chronic liver disease (CLD), resulting in cirrhosis, hepatic failure, and hepatocellular carcinoma. Accurately evaluating liver fibrosis in NAFLD patients is important for identifying those who may progress to severe clinical conditions such as liver cirrhosis and hepatocellular carcinoma [4–7]. Liver biopsies are the gold standard for diagnosing NASH and associated liver fibrosis [8]. However, there is controversy surrounding the active use of liver biopsies for these purposes, because they have several drawbacks [9, 10]. A liver biopsy is highly costly and invasive with rare but potentially life-threatening complications [11]. In addition, sampling errors may occur, because a standard liver biopsy sample represents only 1/50,000 of the whole liver [12]. Furthermore, inter- and intra-observer variability also poses serious problems for the pathological diagnosis of NAFLD [13–17]. Accordingly, there is an urgent need for a non-invasive method for estimating the stage of liver fibrosis in NAFLD patients. Several methods using serum markers [18, 19], scoring systems [20–23], and imaging techniques, such as transient elastography [24–26], have been developed. Although each method has been reported as useful, few have been independently validated. Several problems also remain unaddressed, such as the methods' complexities, reproducibilities, and costs for routine clinical use.

Recently, we developed a new glyco-marker for liver fibrosis using the glycan sugar chain-based immunoassay. The FastLec-Hepa system was used to determine the serum values of sweet-doughnut hyperglycosylated *Wisteria floribunda* agglutinin-positive Mac-2 binding protein (WFA^+-M2BP) for the assessment of liver fibrosis [27–29]. Toshima et al. [30] and Yamasaki et al. [31] reported that this assay offered a feasible means of assessing liver fibrosis in patients with CLD due to the hepatitis C virus (HCV). However, the progressive patterns of fibrosis may differ for CLD due to HCV and CLD due to NAFLD. Indeed, liver specimens from NAFLD patients show pericellular fibrosis around the central vein in the early stages, with gradual progression to fibrosis when central veins become connected to surrounding lobules. In contrast, central vein involvement in patients with CLD due to HCV is generally preceded by portal tract damage with pathological changes to the portal vein.

We investigated the clinical usefulness of serum WFA^+-M2BP values in patients with well-characterized NAFLD. First, we confirmed the efficacy of serum WFA^+-M2BP values for assessing the stage of fibrosis. Second, we compared the diagnostic performances of serum WFA^+-M2BP and other non-invasive fibrosis markers and tests that are used to estimate the stage of liver fibrosis.

Methods

Patients

We retrospectively reviewed 325 NAFLD patients who underwent liver biopsy at Ehime University Hospital (Ehime, Japan), Ikeda Municipal Hospital (Osaka, Japan), Kawasaki Medical School Hospital (Okayama, Japan), or Sapporo Kosei General Hospital (Hokkaido, Japan). The exclusion criteria were as follows: a history of other liver diseases, including hepatitis B virus or HCV infection; administration of drugs that influence the activity of the disease, such as tamoxifen or a glucocorticoid; or a history of alcohol abuse (defined as $\geq$20 g of alcohol daily). Written informed consent was obtained from all patients who participated. The study protocol conformed to the ethical guidelines of the 1975 Declaration of Helsinki, as reflected by each institutional review committee's a priori approval of this study.

Histological evaluation

Each NAFLD patient received a liver biopsy under laparoscopy or ultrasonography between July 2003 and September 2013. The biopsied liver samples were fixed in formalin and were embedded in paraffin according to the standard procedure at each institution. Slices (4 μm thick) were stained with hematoxylin and eosin (H&E), Azan-Mallory, silver, and Elastica van Gieson at Keio University. Liver samples <15 mm long were excluded, because the detection of liver fibrosis may be affected by sampling errors with such samples. A minimum of six portal tracts in the specimen was required for diagnosis. All liver samples were independently evaluated by three experienced liver-specialized pathologists (M.S., G.Y., and M.K.) who were blinded to the clinical data, and all evaluations were validated through discussion. The liver fibrosis stages were

assessed according to Brunt's criteria [32]. Significant and severe fibrosis was defined as ≥stage 2 and ≥stage 3, respectively. Thirty-six patients were excluded because of clinical and/or histological reasons; thus, 289 patients were included in the final analysis.

Clinical and biochemical data

Relevant clinical data were recorded, including the patient's age, sex, weight, and height. Body mass index (BMI) was calculated as weight (kg) divided by height (m) squared. Venous blood samples were obtained in the morning after overnight fasting, either immediately before or no more than 2 months after liver biopsy. The blood samples were stored at −80 °C until analysis.

The biochemical variables were measured using a conventional automated analyzer at the respective hospitals. We analyzed the serum levels for the following: platelet count, prothrombin time, bilirubin, aspartate aminotransferase (AST), alanine aminotransferase (ALT), gamma-glutamyl-transpeptidase, albumin, cholesterol, triglyceride, fasting plasma glucose (FPG), ferritin, and hyaluronic acid. The AST-to-platelet ratio index (APRI) was calculated as follows: [AST (U/L)/UNL × 100]/platelet count. In this equation, UNL is the upper limit of the normal AST [33]. The FIB-4 index was calculated as follows: age (years) × AST (U/L)/platelet count ($\times 10^9$/L) × $\sqrt{\text{ALT}}$ (U/L) [20]. The NAFLD fibrosis score was calculated as follows: $-1.675 + 0.037 \times$ age (years) $+ 0.094 \times$ BMI (kg/m^2) $+ 1.13 \times$ impaired fasting glycemia or diabetes (yes = 1; no = 0) $+ 0.99 \times$ AST/ALT ratio $- 0.013 \times$ platelet ($\times 10^9$/L) $- 0.66 \times$ albumin (g/dL) [21].

Serum *Wisteria floribunda* agglutinin-positive Mac-2 binding protein value

The WFA$^+$-M2BP value in sera was measured by a WFA-antibody immunoassay using a chemiluminescence enzyme immunoassay machine (HISCL-2000i; Sysmex, Kobe, Japan), as previously reported [27, 28, 30, 31]. The measured values of WFA$^+$-M2BP using the conjugated WFA were indexed with the obtained values using the following equation: cutoff index (COI) = ([WFA$^+$-M2BP]$_{\text{sample}}$ − [WFA$^+$-M2BP]$_{\text{NC}}$) ÷ ([WFA$^+$-M2BP]$_{\text{PC}}$) − [WFA$^+$-M2BP]$_{\text{NC}}$). In this equation, [WFA$^+$-M2BP]$_X$ denotes the [WFA + -M2BP] count of the serum sample ($_X$ = sample), positive control ($_X$ = PC), or negative control ($_X$ = NC).

Statistical analysis

Quantitative values are presented as mean ± standard deviation, unless otherwise noted. The Steel–Dwass test was used for multiple comparisons of continuous variables among the different groups. Univariate and multivariate analyses were performed using a logistic regression model. Each cutoff value was determined from the receiver operating characteristic (ROC) curve analyses. The diagnostic performances of the markers were expressed as the diagnostic specificity, sensitivity, positive predictive value, negative predictive value, and area under the ROC (AUROC) curve. p values <0.05 were considered statistically significant. All statistical analyses were performed using JMP, version 11 software (SAS Institute, Tokyo, Japan).

Results

Cross-sectional association between *Wisteria floribunda* agglutinin-positive Mac-2 binding protein values and the fibrosis stage

The patients' characteristics are summarized in Table 1. The mean age of the 289 patients (159 men and 130 women) was 54.8 ± 14.6 years old. Figure 1 shows the serum WFA$^+$-M2BP values for each fibrosis stage. The serum WFA$^+$-M2BP values measured by glycan-based immunoassay ranged from 0.12 to 11.06 (COI). The

Table 1 Patients' clinical characteristics and laboratory data

Features	Total (n = 289)
Male/female	159/130
Age (years)	54.8 ± 14.6
Body mass index (kg/m^2)	27.6 ± 4.7
Platelet count (10^9/l)	18.9 ± 6.8
Prothrombin time (%)	99.3 ± 16.7
Bilirubin (mg/dl)	0.97 ± 0.6
AST (U/l)	61.4 ± 48.9
ALT (U/l)	85.5 ± 68.9
GGT (U/l)	92.3 ± 89.9
Albumin (g/dl)	4.2 ± 0.4
Cholesterol (mg/dl)	195.4 ± 41.1
Triglyceride (mg/dl)	144.4 ± 77.2
FPG (mg/dl)	115.2 ± 38.4
Ferritin (ng/ml)	261.2 ± 258.5
WFA$^+$-M2BP (COI)	1.26 ± 1.44
Fibrosis stage (0/1/2/3/4)	35/113/49/41/51

Values are expressed as mean ± standard deviation

AST aspartate aminotransferase, *ALT* alanine aminotransferase, *COI* cutoff index, *GGT* gamma-glutamyl transpeptidase, *FPG* fasting plasma glucose, WFA$^+$-*M2BP Wisteria floribunda* agglutinin-positive Mac-2 binding protein

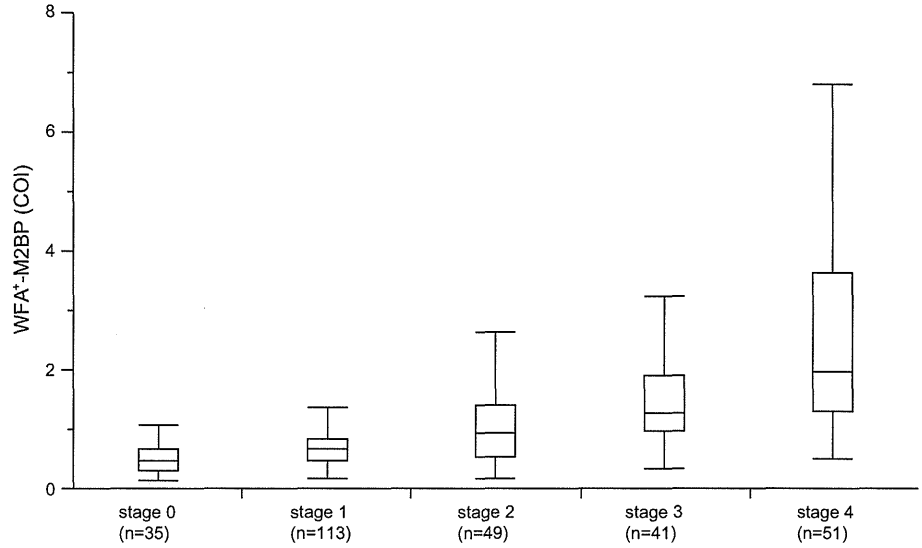

Fig. 1 The serum *Wisteria floribunda* agglutinin-positive Mac-2 binding protein (WFA^+-M2BP) values for each fibrosis stage. The *top* and *bottom* of each *box* represent the first and third quartiles, respectively, with the height of the box representing the interquartile range, covering 50 % of the values. The *line* across each *box* represents the median. The *whiskers* show the highest and lowest values. All pairs of groups are significantly different, as assessed using the Steel–Dwass test ($p < 0.01$). *COI* cutoff index

Table 2 Variables associated with the fibrosis stage according to multivariate regression analyses

	Stage 0 vs. stages 1–4		Stages 0–1 vs. stages 2–4		Stages 0–2 vs. stages 3–4		Stages 0–3 vs. stage 4	
	Odds ratio (95 % CI)	*p* value	Odds ratio (95 % CI)	*p* value	Odds ratio (95 % CI)	*p* value	Odds ratio (95 % CI)	*p* value
Age (years)			1.049 (1.014–1.087)	0.006				
BMI (kg/m^2)	1.228 (1.089–1.412)	0.002						
Platelet count (10^9/L)					0.864 (0.787–0.941)	0.001	0.895 (0.814–0.978)	0.017
Prothrombin time (%)	0.948 (0.914–0.982)	0.004	0.957 (0.925–0.986)	0.007			0.963 (0.927–0.993)	0.028
AST (U/l)	1.078 (1.023–1.144)	0.008	1.036 (1.022–1.052)	<0.001				
FPG (mg/dl)			1.013 (1.004–1.024)	0.007	1.014 (1.004–1.024)	0.004	1.012 (1.002–1.022)	0.013
WFA^+-M2BP (COI)			5.875 (2.339–16.369)	<0.001	8.471 (3.562–22.725)	<0.001	2.390 (1.463–4.423)	0.002

CI confidence interval, *BMI* body mass index, *AST* aspartate aminotransferase, *FPG* fasting plasma glucose, WFA^+-*M2BP Wisteria floribunda* agglutinin-positive Mac-2 binding protein, *COI* cutoff index

WFA^+-M2BP value in patients with stages 0 ($n = 35$), 1 ($n = 113$), 2 ($n = 49$), 3 ($n = 41$), and 4 ($n = 51$) of fibrosis had COIs of 0.57, 0.70, 1.02, 1.57, and 2.96, respectively, demonstrating a stepwise increase with an increasing severity of liver fibrosis (Fig. 1). All pairs of groups differed significantly according to the Steel–Dwass test (stage 0 vs. stage 1, $p = 0.012$; stage 0 vs. stage 2, $p < 0.001$; stage 0 vs. stage 3, $p < 0.001$; stage 0 vs. stage 4, $p < 0.001$; stage 1 vs. stage 2, $p = 0.002$; stage 1 vs. stage 3, $p < 0.001$; stage 1 vs. stage 4, $p < 0.001$; stage 2 vs. stage 3, $p = 0.014$; stage 2 vs. stage 4, $p < 0.001$; and stage 3 vs. stage 4, $p = 0.008$).

Comparisons of variables associated with the diagnosis of the fibrosis stage

The variables associated with each stage of liver fibrosis were assessed by univariate and multivariate analyses (Tables S1, 2).

Variables associated with the presence of fibrosis (≥stage 1)

According to univariate analysis, eight variables (age, BMI, platelet count, prothrombin time, AST, ALT,

albumin, and the WFA^+-M2BP value) were associated with the presence of fibrosis (Table S1). Multivariate analysis showed that the BMI [odds ratio (OR) 1.228, 95 % confidence interval (CI) 1.089–1.412], prothrombin time (OR 0.948; 95 % CI 0.914–0.982), and AST (OR 1.078; 95 % CI 1.023–1.144) were independently associated with the presence of fibrosis (Table 2).

Variables associated with the presence of significant fibrosis (≥stage 2)

Univariate analysis identified ten variables (sex, age, platelet count, prothrombin time, bilirubin, AST, albumin, cholesterol, FPG, and the WFA^+-M2BP value) that were associated with the presence of significant fibrosis (Table S1). However, multivariate analysis showed that age (OR 1.049; 95 % CI 1.014–1.087), prothrombin time (OR 0.957; 95 % CI 0.925–0.986), AST (OR 1.036; 95 % CI 1.022–1.052), ALT (OR 1.036; 95 % CI 1.022–1.052), FPG (OR 1.013; 95 % CI 1.004–1.024), and the WFA^+-M2BP value (OR 5.875; 95 % CI 2.339–16.369) were independently associated with the presence of significant fibrosis (Table 2).

Variables associated with the presence of severe fibrosis (≥stage 3)

According to univariate analysis, ten variables (sex, age, platelet count, prothrombin time, bilirubin, albumin, cholesterol, triglyceride, FPG, and the WFA^+-M2BP value) were associated with the presence of severe fibrosis (Table S1). However, multivariate analysis showed that the platelet count (OR 0.864; 95 % CI 0.787–0.941), FPG (OR 1.014; 95 % CI 1.004–1.024), and the WFA^+-M2BP value (OR 8.471; 95 % CI 3.562–22.725) were independently associated with the presence of severe fibrosis (Table 2).

Variables associated with the presence of cirrhosis (stage 4)

Univariate analysis identified 11 variables (sex, age, platelet count, prothrombin time, bilirubin, ALT, albumin, cholesterol, triglyceride, FPG, and the WFA^+-M2BP value) that were associated with the presence of cirrhosis (Table S1). Multivariate analysis identified that the platelet count (OR 0.895; 95 % CI 0.814–0.978), prothrombin time (OR 0.963; 95 % CI 0.927–0.993), FPG (OR 1.012; 95 % CI 1.002–1.022), and the WFA^+-M2BP value (OR 2.390; 95 % CI 1.462–4.423) were independently associated with the presence of cirrhosis (Table 2).

Diagnostic power of the *Wisteria floribunda* agglutinin-positive Mac-2 binding protein values for each fibrosis stage

The WFA^+-M2BP ROC curves for diagnosing each fibrosis stage are presented in Fig. 2. The AUROC curve values (95 % CI) for the prediction of ≥stage 1, ≥stage 2, ≥stage 3, and stage 4 using the serum WFA^+-M2BP values were 0.788 (0.736–0.833), 0.838 (0.790–0.879), 0.876 (0.832–0.911), and 0.879 (0.835–0.914), respectively (Table 3). The optimal cutoff values were 0.59 for ≥stage 1, 0.90 for ≥stage 2, 0.94 for ≥stage 3, and 1.46 for stage 4 (Table 3). The sensitivities for the prediction of ≥stage 1, ≥stage 2, ≥stage 3, and stage 4 were 74.8, 77.3, 85.9, and 72.6 %, respectively; whereas, the specificities were 74.3, 81.1, 74.6, and 87.0 %, respectively (Table 3).

Comparisons of AUROC curve values for diagnosing the fibrosis stage

The AUROC curve values for diagnosing each fibrosis stage are shown in Table 4. Compared with the other surrogate markers and scoring systems, the serum WFA^+-M2BP was the most useful marker for differentiating stages 0–2 from stages 3–4 and stages 0–3 from stage 4. The AUROC curve values for differentiating stages 0–1 from stages 2–4 were compatible with the serum WFA^+-M2BP (0.838), hyaluronic acid (0.833), and the FIB-4 index (0.844).

Discussion

Clinically, it is very important to identify patients who have NASH with advanced fibrosis, because these patients have more liver-related complications and a greater mortality rate than patients who have NASH without liver fibrosis [4–7]. Although a liver biopsy is the gold standard for diagnosing and assessing the stages of fibrosis, research on noninvasive methods for assessing the fibrosis stages have rapidly evolved over the last decade [17–26]. In this study, we found that the serum WFA^+-M2BP values measured using a glycan-based immunoassay provided a useful diagnostic factor for assessing the liver fibrosis stage in NAFLD patients (Fig. 1). The glycan-based immunoassay was previously developed as a simple system for automatically detecting unique fibrosis-related glycoalterations [27–31]. Moreover, the accuracy of the serum WFA^+-M2BP values for diagnosing severe fibrosis and cirrhosis was superior to that offered by other surrogate markers and tests (Table 4).

M2BP is a secreted glycoprotein that is found in the serum of healthy individuals, but its concentration

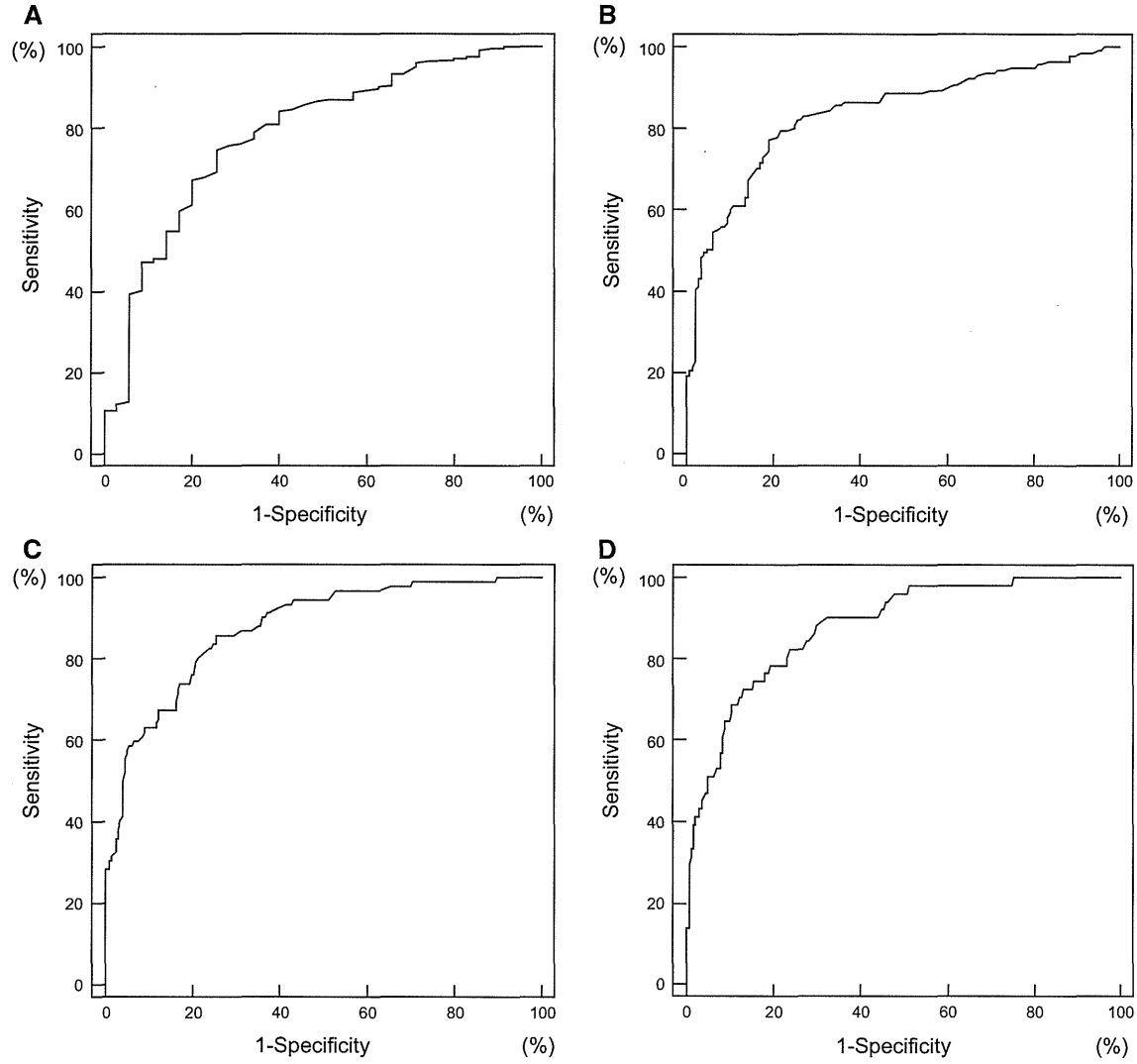

Fig. 2 The diagnostic capabilities of the serum *Wisteria floribunda* agglutinin-positive Mac-2 binding protein (WFA^+-M2BP) values for assessing the stage of liver fibrosis. The areas under the receiver operating characteristic curve of serum WFA^+-M2BP for diagnosing liver fibrosis were as follows: **a** 0.788 for stage ≥1; **b** 0.838 for stage ≥2; **c** 0.876 for stage ≥3; and **d** 0.879 for stage 4

increases in patients with various cancers and viral infections, including HCV [34, 35]. This protein binds galectin-3, β-1 integrins, collagens, and fibronectin and has some relevance to cell–cell and cell–extracellular matrix adhesion [36, 37]. Therefore, it is reasonable to assume that M2BP reflects the progression of fibrosis in cases of CLD. Indeed, using proteome analysis, Cheung et al. [38] found that serum M2BP is a potential marker of fibrosis progression in HCV patients.

In this study, we found that the serum WFA^+-M2BP value can be used to distinguish the fibrosis stages in NAFLD patients (Fig. 1; Tables S1, 2, 3). Recently, Kamada et al. [39] reported that the serum M2BP value (the whole M2BP protein measured by enzyme-linked immunosorbent assay) can be used for predicting the fibrosis stage in NAFLD patients. However, there are several differences between the present study and Kamada et al.'s study. In our study, the serum WFA^+-M2BP value (the altered M2BP with fibrosis-related *N*-glycans measured by glycan-based immunoassay) increased stepwise with the increasing severity of liver fibrosis, whereas a stepwise increase was not found in Kamada et al.'s study. Further, our method can distinguish between the fibrosis stages more clearly, not only in patients with advanced fibrosis stage but also in those with earlier fibrosis stages of NAFLD (Fig. 1). In our previous study [27], we found that both the quantity and quality of M2BP were altered during the progression of fibrosis of CLD due to HCV. Since the *N*-glycosylation of M2BP was dramatically altered during the progression of liver fibrosis, we considered that the

Table 3 Serum *Wisteria floribunda* agglutinin-positive Mac-2 binding protein values for assessing liver fibrosis

Stage	AUC (95 % CI)	Cutoff level	Sensitivity (%)	Specificity (%)	PPV (%)	NPV (%)	Predictive accuracy (%)
≥Stage 1	0.788 (0.736–0.833)	0.59	74.8	74.3	95.5	28.9	74.7
≥Stage 2	0.838 (0.790–0.879)	0.90	77.3	81.1	79.6	78.9	79.2
≥Stage 3	0.876 (0.832–0.911)	0.94	85.9	74.6	61.2	91.9	78.2
Stage 4	0.879 (0.835–0.914)	1.46	72.6	87.0	54.4	93.7	84.4

AUC area under receiver operating characteristic curve, *CI* confidence interval, *PPV* positive predictive value, *NPV* negative predictive value

Table 4 Comparisons of the areas under the receiver operating characteristic curves for each fibrosis marker and scoring system

Marker and score	≥Stage 1	≥Stage 2	≥Stage 3	Stage 4
WFA^+-M2BP	0.788	0.838	0.876	0.879
Platelet count	0.649	0.719	0.810	0.815
Hyaluronic acid	0.757	0.833	0.856	0.858
AST/ALT ratio	0.607	0.733	0.770	0.752
APRI	0.867	0.804	0.758	0.745
FIB-4 index	0.793	0.844	0.857	0.849
NAFLD fibrosis score	0.766	0.811	0.808	0.824

WFA^+-*M2BP Wisteria floribunda* agglutinin-positive Mac-2 binding protein, *AST* aspartate aminotransferase, *ALT* alanine aminotransferase, *APRI* AST-to-platelet ratio index, *NAFLD* non-alcoholic fatty liver disease

WFA^+-M2BP reflects the fibrosis status more precisely than the whole M2BP protein. Further, the quantification of the WFA^+-M2BP may offer a better marker for assessing the liver fibrosis stage than does the quantification of the M2BP protein. Currently, the *N*-glycan structures of WFA^--M2BP and WFA^+-M2BP are being analyzed using mass spectrometry in our laboratory. Moreover, our system has been converted to a fully automated immunoassay analyzer for clinical use, featuring a measurement time of only 17 min, which has clear practical implications [27, 28, 30, 31].

Numerous non-invasive panels of the tests have been developed to assess the liver fibrosis stages [17–26]. In this study, the serum WFA^+-M2BP values offered a superior AUROC curve for the diagnosis of severe fibrosis and cirrhosis compared with the FIB-4 index and five other markers and scoring systems (Table 4). In a study of a large Japanese cohort, the FIB-4 index was the most useful index for diagnosing patients with advanced fibrosis [40]. Although the American Association for the Study Liver Diseases' guidelines [3] recommend the NAFLD fibrosis score [21] when deciding whether to perform a liver biopsy, the usefulness of this score remains questionable in Asian patients [40, 41]. Consistent with these studies, the NAFLD fibrosis score yielded lower AUROCs than the WFA^+-M2BP values and the FIB-4 index for diagnosing fibrosis in our cohort (Table 4).

There are two main strengths of the present study's cohort. First, the sample size ($n = 289$) was relatively large, and the patients' clinical backgrounds were well characterized. Second, the pathological diagnoses were performed and validated by three experienced liver-specific pathologists. Currently, the definitive diagnosis of NAFLD and the distinction of its phenotypes rely on the pathologist's interpretation of the liver biopsy [8]; therefore, an accurate and reproducible consensus regarding the pathological findings is necessary for diagnosing NAFLD. However, in practice, the interpretation of NAFLD's histology varies substantially. In this study, we excluded patients whose liver samples were inadequate for histological evaluation (e.g., because of insufficient sample size). Moreover, the considerable rate of inter-observer variation is one of the major problems in the histological diagnosis of NAFLD [13–17]. Our strategy mainly focused on reducing this variation, and our study may provide a reliable cohort for identifying surrogate markers and for investigating the management of NAFLD patients.

This study also has several limitations. First, we investigated the usefulness of the serum WFA^+-M2BP values in a cross-sectional study. Therefore, the use of the serum WFA^+-M2BP values for monitoring natural history, predicting outcomes, and predicting responses to therapeutic interventions remain unknown. In fact, the prevalence of NAFLD is high among individuals with diabetes or dyslipidemia [1–3], and some patients have already managed their condition through lifestyle interventions and/or medication at the time of liver biopsy. Further prospective studies are necessary to address these issues. In addition, since the biochemical analyses were performed separately at the respective hospitals, any variations among each institution cannot be ruled out. Moreover, several selection

biases may be present, because all the patients had been diagnosed and had received liver biopsies at hepatology centers, which may have caused referral bias. Therefore, validation studies are necessary in the general population.

In conclusion, the measurement of the serum WFA^+-M2BP values using a glycan-based immunoassay provides an accurate and reliable method for assessing the liver fibrosis stage in NAFLD patients. This method appears quite promising as a means for evaluating the natural course of the disease, therapeutic effects, and the suitability of liver biopsies.

Acknowledgments This study was supported by a Grant-in-Aid from the Ministry of Health, Labour, and Welfare of Japan. This research was performed by the Hepatitis Glyco-biomarker Study Group.

Conflict of interest The authors declare that they have no conflict of interest.

References

1. Angulo P. Nonalcoholic fatty liver disease. N Engl J Med. 2002;346:1221–31.
2. Bhala N, Usherwood T, George J. Non-alcoholic fatty liver disease. BMJ. 2009;339:b2474.
3. Chalasani N, Younossi Z, Lavine JE, et al. The diagnosis and management of non-alcoholic fatty liver disease: practice guideline by the American Association for the Study of Liver Diseases, American College of Gastroenterology, and the American Gastroenterological Association. Hepatology. 2012;55:2005–23.
4. Adams LA, Lymp JF, StSauver J, et al. The natural history of nonalcoholic fatty liver disease: a population-based cohort study. Gastroenterology. 2005;129:113–21.
5. Hui JM, Kench JG, Chitturi S, et al. Long-term outcomes of cirrhosis in nonalcoholic steatohepatitis compared with hepatitis C. Hepatology. 2003;38:420–7.
6. Yasui K, Hashimoto E, Komorizono Y, et al. Characteristics of patients with nonalcoholic steatohepatitis who develop hepatocellular carcinoma. Clin Gastroenterol Hepatol. 2011;9:428–33.
7. Bhala N, Angulo P, van der Poorten D, et al. The natural history of nonalcoholic fatty liver disease with advanced fibrosis or cirrhosis: an international collaborative study. Hepatology. 2011;54:1208–16.
8. Brunt EM. Pathology of nonalcoholic fatty liver disease. Nat Rev Gastroenterol Hepatol. 2010;7:195–203.
9. Laurin J. Motion—all patients with NASH need to have a liver biopsy: arguments against the motion. Can J Gastroenterol. 2002;16:722–6.
10. Sumida Y, Nakajima A, Itoh Y. Limitations of liver biopsy and non-invasive diagnostic tests for the diagnosis of nonalcoholic fatty liver disease/nonalcoholic steatohepatitis. World J Gastroenterol. 2014;20:475–85.
11. Cadranel JF, Rufat P, Degos F. Practices of liver biopsy in France: results of a prospective nationwide survey. Hepatology. 2000;32:477–81.
12. Ratziu V, Charlotte F, Heurtier A, et al. Sampling variability of liver biopsy in nonalcoholic fatty liver disease. Gastroenterology. 2005;128:1898–906.
13. Younossi ZM, Gramlich T, Liu YC, et al. Nonalcoholic fatty liver disease: assessment of variability in pathologic interpretations. Mod Pathol. 1998;11:560–5.
14. Kleiner DE, Brunt EM, Van Natta M, et al. Design and validation of a histological scoring system for nonalcoholic fatty liver disease. Hepatology. 2005;41:1313–21.
15. Fukusato T, Fukushima J, Shiga J, et al. Interobserver variation in the histopathological assessment of nonalcoholic steatohepatitis. Hepatol Res. 2005;33:122–7.
16. Miyaoka H, Michitaka K, Tokumoto Y, et al. Laparoscopic features and interobserver variation of histological diagnosis in patients with non-alcoholic fatty liver disease. Dig Endosc. 2008;20:22–8.
17. Gawrieh S, Knoedler DM, Saeian K, et al. Effects of interventions on intra- and interobserver agreement on interpretation of nonalcoholic fatty liver disease histology. Ann Diagon Pathol. 2011;15:19–24.
18. Suzuki A, Angulo P, Lymp J, et al. Hyaluronic acid, an accurate serum marker for severe hepatic fibrosis in patients with non-alcoholic fatty liver disease. Liver Int. 2005;25:779–86.
19. Yoneda M, Mawatari H, Fujita K, et al. Type IV collagen 7 s domain is an independent clinical marker of the severity of fibrosis in patients with nonalcoholic steatohepatitis before the cirrhotic stage. J Gastroenterol. 2007;42:375–81.
20. Vallet-Pichard A, Mallet V, Nalpas B, et al. FIB-4: an inexpensive and accurate marker of fibrosis in HCV infection. Comparison with liver biopsy and fibrotest. Hepatology. 2007;46:32–6.
21. Angulo P, Hui JM, Marchesini G, et al. The NAFLD fibrosis score: a noninvasive system that identifies liver fibrosis in patients with NAFLD. Hepatology. 2007;45:846–54.
22. Harrison SA, Oliver D, Arnold HL, et al. Development and validation of a simple NAFLD clinical scoring system for identifying patients without advanced disease. Gut. 2008;57:1441–7.
23. Guha IN, Parkes J, Roderick P, et al. Noninvasive markers of fibrosis in nonalcoholic fatty liver disease: validating the European Liver Fibrosis Panel and exploring simple markers. Hepatology. 2008;47:455–60.
24. Wong VW, Vergniol J, Wong GL, et al. Diagnosis of fibrosis and cirrhosis using liver stiffness measurement in nonalcoholic fatty liver disease. Hepatology. 2010;51:454–62.
25. Yoneda M, Suzuki K, Kato S, et al. Nonalcoholic fatty liver disease: US-based acoustic radiation force impulse elastography. Radiology. 2010;256:640–7.
26. Ochi H, Hirooka M, Koizumi Y, et al. Real-time tissue elastography for evaluation of hepatic fibrosis and portal hypertension in nonalcoholic fatty liver diseases. Hepatology. 2012;56:1271–8.
27. Kuno A, Ikehara Y, Tanaka Y, et al. A serum "sweet-doughnut" protein facilitates fibrosis evaluation and therapy assessment in patients with viral hepatitis. Sci Rep. 2013;3:1065.
28. Kuno A, Sato T, Shimazaki H, et al. Reconstruction of a robust glycodiagnostic agent supported by multiple lectin-assisted glycan profiling. Proteomics Clin Appl. 2013. doi:10.1002/prca.201300010.
29. Ito K, Kuno A, Ikehara Y, et al. LecT-Hepa, a glyco-marker derived from multiple lectins, as a predictor of liver fibrosis in chronic hepatitis C patients. Hepatology. 2012;56:1448–56.
30. Toshima T, Shirabe K, Ikegami T, et al. A novel serum marker, glycosylated *Wisteria floribunda* agglutinin-positive Mac-2 binding protein (WFA^+-M2BP), for assessing liver fibrosis. J Gastroenterol. 7 Mar 2014 (Epub ahead of print).
31. Yamasaki K, Tateyama M, Abiru S, et al. Elevated serum levels of *Wisteria floribunda agglutinin*-positive human Mac-2 binding protein predict the development of hepatocellular carcinoma in hepatitis C patients. Hepatology. 12 Jul 2014. doi: 10.1002/hep.27305. (Epub ahead of print).
32. Brunt EM, Janney CG, Di Bisceglie AM, et al. Nonalcoholic steatohepatitis: a proposal for grading and staging the histological lesions. Am J Gastroenterol. 1999;94:2467–74.

33. Wai CT, Greenson JK, Fontana RJ, et al. A simple noninvasive index can predict both significant fibrosis and cirrhosis in patients with chronic hepatitis C. Hepatology. 2003;38:518–26.
34. Iacobelli S, Arnò E, D'Orazio A, et al. Detection of antigens recognized by a novel monoclonal antibody in tissue and serum from patients with breast cancer. Cancer Res. 1986;46:3005–10.
35. Artini M, Natoli C, Tinari N, et al. Elevated serum levels of 90 K/MAC-2 BP predict unresponsiveness to alpha-interferon therapy in chronic HCV hepatitis patients. J Hepatol. 1996;25:212–7.
36. Inohara H, Akahani S, Koths K, et al. Interactions between galectin-3 and Mac-2 binding protein mediate cell-cell adhesion. Cancer Res. 1996;56:4530–4.
37. Sasaki T, Brakebusch C, Engel J, et al. Mac-2 binding protein is a cell-adhesive protein of the extracellular matrix which self-assembles into ring-like structures and binds beta1 integrins, collagens and fibronectin. EMBO J. 1998;17:1606–13.
38. Cheung KJ, Tilleman K, Deforce D, et al. The HCV serum proteome: a search for fibrosis protein markers. J Viral Hepat. 2009;16:418–29.
39. Kamada Y, Fujii H, Fujii H, et al. Serum Mac-2 binding protein levels as a novel diagnostic biomarker for prediction of disease severity and nonalcoholic steatohepatitis. Proteomics Clin Appl. 14 June 2013. doi: 10.1002/prca.201200137. (Epub ahead of print).
40. Sumida Y, Yoneda M, Hyogo H, et al. Validation of the FIB4 index in a Japanese nonalcoholic fatty liver disease population. BMC Gastroenterol. 2012;12:2.
41. Wong VW, Wong GL, Chim AM, et al. Validation of the NAFLD fibrosis score in a Chinese population with low prevalence of advanced fibrosis. Am J Gastroenterol. 2008;103:1682–8.

Liver INTERNATIONAL
OFFICIAL JOURNAL OF THE INTERNATIONAL ASSOCIATION FOR THE STUDY OF THE LIVER

Liver International ISSN 1478-3223

ORIGINAL ARTICLE

Branched-chain amino acids reduce hepatic iron accumulation and oxidative stress in hepatitis C virus polyprotein-expressing mice

Masaaki Korenaga[1,2], Sohji Nishina[1], Keiko Korenaga[1], Yasuyuki Tomiyama[1], Naoko Yoshioka[1], Yuichi Hara[1], Yusuke Sasaki[3], Yasushi Shimonaka[3] and Keisuke Hino[1]

1 Department of Hepatology and Pancreatology, Kawasaki Medical School, Okayama, Japan
2 The Research Center for Hepatitis and Immunology, National Center for Global Health and Medicine (NCGM), Chiba, Japan
3 Product Research Department, Chugai Pharmaceutical Co., Kanagawa, Japan

Keywords
hepatitis C virus – hepatic mitochondrial dysfunction – hepcidin-25 – iron metabolic disorder – reactive oxygen species

Abbreviations
BAP, biological antioxidant potential; BCAA, branched-chain amino acids; BTR, ratio of BCAA relative to tyrosine; CHOP, CCAAT/enhancer-binding protein homology protein; CPT I, carnitine palmitoyl transferase I; dROM, derivatives of reactive oxygen metabolites; HCC, hepatocellular carcinoma; HCV, hepatitis C virus; HCVTgM, transgenic mice expressing hepatitis C virus polyprotein; ROS, reactive oxygen species; SOD2, superoxide dismutase 2; SREBP, sterol regulatory element-binding protein.

Correspondence
Masaaki Korenaga MD, PhD,The Research Center for Hepatitis and Immunology, National Center for Global Health and Medicine (NCGM), 1-7-1 Kohnodai, Ichikawa Chiba, Japan
Tel: 81 47 372 3501
Fax: 81 47 375 4766
e-mail: dmkorenaga@hospk.ncgm.go.jp

Received 4 March 2014
Accepted 16 August 2014

DOI:10.1111/liv.12675

Abstract

Background & Aims: Branched-chain amino acids (BCAA) reduce the incidence of hepatocellular carcinoma (HCC) in patients with cirrhosis. However, the mechanisms that underlie these effects remain unknown. Previously, we reported that oxidative stress in male transgenic mice that expressed hepatitis C virus polyprotein (HCVTgM) caused hepatic iron accumulation by reducing hepcidin transcription, thereby leading to HCC development. This study investigated whether long-term treatment with BCAA reduced hepatic iron accumulation and oxidative stress in iron-overloaded HCVTgM and in patients with HCV-related advanced fibrosis. *Methods:* Male HCVTgM were fed an excess-iron diet that comprised either casein or 3.0% BCAA, or a control diet, for 6 months. *Results:* For HCVTgM, BCAA supplementation increased the serum hepcidin-25 levels and antioxidant status [ratio of biological antioxidant potential (BAP) relative to derivatives of reactive oxygen metabolites (dROM)], decreased the hepatic iron contents, attenuated reactive oxygen species generation, and restored mitochondrial superoxide dismutase expression and mitochondrial complex I activity in the liver compared with mice fed the control diet. After 48 weeks of BCAA supplementation in patients with HCV-related advanced fibrosis, BAP/dROM and serum hepcidin-25 increased and serum ferritin decreased compared with the pretreatment levels. *Conclusions:* BCAA supplementation reduced oxidative stress by restoring mitochondrial function and improved iron metabolism by increasing hepcidin-25 in both iron-overloaded HCVTgM and patients with HCV-related advanced fibrosis. These activities of BCAA may partially account for their inhibitory effects on HCC development in cirrhosis patients.

Hepatitis C virus (HCV) causes acute and chronic hepatitis, cirrhosis, and hepatocellular carcinoma (HCC) (1). New direct-acting antiviral treatments are expected to eliminate this virus in about 90% of patients (2), but therapies that could reduce disease progression in chronically infected individuals would be highly beneficial.

Valine, leucine and isoleucine are essential branched-chain amino acids (BCAA). A decreased ratio of serum

BCAA relative to aromatic amino acids, a hallmark of cirrhosis, is caused by several factors, including reduced nutritional intake and ammonia detoxification in skeletal muscles (3). BCAA supplementation can improve the nutritional status and albumin synthesis by activating the mammalian target of rapamycin signalling cascade (4, 5) and glucose metabolism in skeletal muscles (6, 7). Long-term oral BCAA supplementation decreases the frequency of HCC in male obese patients with cirrhosis (8). BCAA also had an antihepatocarcinogenic activity in an animal model of insulin resistance (9, 10). In addition, glucose intolerance is closely linked to hepatocarcinogenesis. However, the mechanisms that underlie these effects remain unknown.

Hepatic oxidative stress and iron overload have been implicated in liver injury and hepatocarcinogenesis in HCV-associated chronic liver diseases (11, 12). The HCV core protein inhibits mitochondrial complex I and generates reactive oxygen species (ROS) *in vivo* (13). Previously, we reported that HCV-induced ROS increases the hepatic iron concentration by reducing hepcidin transcription in transgenic mice that express HCV polyprotein (14), where even modest iron supplementation in these mice resulted in the development of liver tumours, including HCC, because of mitochondrial injury (15). Thus, hepatic iron overload and oxidative stress via mitochondrial injury are critical during HCC pathogenesis.

In the present study, we examined whether long-term BCAA supplementation could prevent the development of hepatic iron accumulation and oxidative stress in HCV transgenic mice fed an excess-iron diet and in patients with HCV-related advanced fibrosis.

Materials and methods

Animals and experimental design

The pAlbSVPA-HCV transgene contains the full-length HCV polyprotein-coding region under the control of the murine albumin promoter/enhancer (16, 17). HCV polyprotein is processed into individual proteins in the liver and expressed at biologically relevant levels in FL-N/35 transgenic mice (HCVTgM) (17). In the present study, male HCVTgM (8 weeks old) were fed a normal rodent diet, including carbonyl iron (45 mg/kg; control, $n = 6$), or an excess-iron diet (carbonyl iron, 225 mg/kg) that contained either 3.0% BCAA (BCAA/iron; $n = 5$) or casein (casein/iron; $n = 7$). Six months later, the mice were sacrificed by CO_2 asphyxiation after a 12-h fast, according to the criteria outlined in the Guide for the Care and Use of Laboratory Animals.

Clinical chemistry tests

The serum concentrations of alanine aminotransferase, aspartate aminotransferase (AST), albumin, glucose, insulin, BCAA, tyrosine and hepcidin-25 were determined in blood samples collected from the inferior vena cava of sacrificed mice at 12 h after fasting. The blood glucose levels were periodically measured using a glucometer (OneTouch Ultra, Lifescan, Inc., Milpitas, CA, USA). The serum insulin levels were measured using an ultrasensitive mouse insulin ELISA kit (Morinaga Milk, Kanagawa, Japan). The serum hepcidin-25 levels were determined by LC/MS/MS (18).

Hepatic iron and triglyceride contents

The hepatic iron concentrations were measured by atomic absorption spectrometry, as described previously (15). The liver tissue was homogenized and the lipids were extracted (19), and the triglyceride levels were measured using a TGE-test Wako kit (Wako Pure Chemicals, Tokyo, Japan), according to the manufacturer's instructions. The protein concentrations were determined by the Lowry method (20) using a DC protein assay kit (Bio-Rad Laboratories, Hercules, CA, USA).

In situ ROS detection

In situ liver ROS production was assessed by staining with dihydroethidium (Invitrogen Corp., Carlsbad, CA, USA), as described previously (14). Dihydroethidium is oxidized to ethidium bromide in the presence of ROS, which stains the nuclei bright red via DNA intercalation (21). The intensity of the fluorescence was quantified using the NIH Image analysis program in three randomly selected areas of the digital images for each mouse.

Derivatives of reactive oxygen metabolites and biological antioxidant potential levels

The derivatives of reactive oxygen metabolites (dROM) and biological antioxidant potential (BAP) levels were measured using a Free Radical Elective Evaluator (Wismerll Co. Ltd, Tokyo, Japan) (22, 23). The dROM measurements were determined based on the ability of transition metals to catalyse the formation of coloured free radicals (detection at 505 nm). The results were expressed in Cartelli units (U.CARR), where 1 U.CARR = 0.8 mg/L of H_2O_2. To obtain the BAP measurements, the blood samples were added to a solution containing $FeCl_3$ bound to a chromogenic substrate (AT, a derivative of thiocyanate). Fe^{3+} reduction to Fe^{2+} caused a chromatic change that was directly proportional to the plasma ROS reduction, which was measured at 505 nm using a photometer. Blood aliquots (10 µl) were mixed with the $FeCl_3$ solution and incubated for 5 min at 37°C before the photometric analysis.

Histological staining

Part of each liver sample was snap-frozen immediately in liquid nitrogen to determine the hepatic triglycerides

and iron concentration. The remaining liver tissue was fixed in 4% paraformaldehyde in phosphate-buffered saline and embedded in paraffin for use in the histological analysis. The liver sections were stained with haematoxylin and eosin.

Real-time reverse transcriptase-PCR

One-step real-time real-time reverse transcriptase-PCR (RT-PCR) was performed, as described previously (14), where the results were expressed as the hepcidin, interleukin 6 (IL6), BMP6 and superoxide dismutase 2 (SOD2) gene mRNA levels relative to β-actin mRNA.

Extraction of nuclear and histone deacetylase activity assay

For isolation of nuclear proteins from mice liver, Nuclear Extraction Kit 1 (Epigentek, Farmingdale, NY, USA) was used. Histone deacetylase (HDAC) activity was assessed using HDAC Activity/Inhibition Direct Assay Kit (Epigentek) according to the manufacturer's instruction.

Isolation of mitochondria and complex I activity determination

Liver mitochondria were isolated and the activity of complex I was assayed (at 25°C) as described previously (3, 24).

Protein extraction and Western blotting

The liver lysate and mitochondrial lysate proteins were separated by sodium dodecyl sulphate-polyacrylamide gel electrophoresis. These proteins were then transferred to polyvinylidene difluoride membranes (Millipore, Bedford, MA, USA) and blocked overnight at 4°C with 1–3% skim milk and 0.1% Tween 20 in Tris-buffered saline, which was followed by incubation at room temperature for 1 h with a primary antibody. Anti-rabbit carnitine palmitoyl transferase I (CPT I), anti-rabbit CPT II (Alpha Diagnostic International, San Antonio, TX, USA), anti-rabbit SREBP1 (Santa Cruz Biotechnology Inc., Santa Cruz, CA, USA), or anti-bacterially expressed mouse CCAAT/enhancer-binding protein homology protein (CHOP) fusion protein (Abcam, Cambridge, England) were used for the liver lysate proteins. Anti-SOD2 (Abcam), anti-Grp75 (mitochondrial heat shock protein70; Abcam), or anti-NDUFB8 (mitochondrial complex I) antibody (Abcam) were used for the mitochondrial lysates. The proteins were blocked for 1 h at room temperature and then incubated overnight at 4°C with a Phospho-stat3 (pSTAT3) antibody (Cell Signaling Technology Inc., Danvers, MA, USA) and a Phospho-Smad1/Smad5/Smad8 (pSMAD1/5/8) antibody (Cell Signaling Technology Inc.).The anti-acetyl-histoneH3K9 and anti-histoneH3 (Cell Signaling Technology Inc,) were used for the nuclear lysates.

Human BCAA supplementation study design

We screened 68 HCV RNA-positive patients who were aged >65 years (Fig. S1). We enrolled 25 patients with HCV-related advanced fibrosis who satisfied the following criteria: serum albumin = 3.5–4.2 g/dl; platelet counts $<15 \times 10^4/\mu l$; amino acid imbalance [based on the ratio of BCAA relative to tyrosine (BTR) <4.40, which was lower than the normal limits]; and no HCC or symptoms of chronic liver failure such as ascites, varices or hepatic encephalopathy. Advanced fibrosis defined liver specimens (METAVIR fibrosis staging: >F3,4) or Fib-4 index (>3.25). The patients were assigned randomly to receive BCAA supplementation (BCAA group; $n = 12$) or follow-up without treatment (non-BCAA group; $n = 13$). BCAA group were given a 4 g BCAA preparation (LIVACT Granules; Ajinomoto, Tokyo, Japan) administered orally three times daily after meals. We measured the plasma oxidized/reduced albumin and serum dROM and BAP as oxidative stress markers at 12, 24 and 48 weeks after starting the treatment. We also measured the levels of serum iron, ferritin, transferrin saturation (TSAT) and hepcidin-25 to evaluate the oxidative stress-associated iron metabolism. Moreover, type IV collagen 7s, type III procollagen peptide (PIIP) and Fib-4 index were measured to confirm the degree of hepatic fibrosis.

Written informed consent was obtained from each study participant. This study was conducted in accordance with the provisions of the 1975 Declaration of Helsinki and it was approved by the Institutional Ethics Committee of Kawasaki Medical School.

Statistical analysis

The results were expressed as mean ± SD. The group results were compared using Levene's or Welch's tests. The changes in the levels of the iron metabolism and oxidative stress markers between the BCAA and the non-BCAA groups were analysed using Wilcoxon rank-sum tests. Pearson's product moment correlation coefficient was used to assess associations between the dihydroethidium-positive areas and the BAP and dROM ratios. Differences were considered statistically significant at $P < 0.05$. The statistical analyses were performed using SPSS software (IBM SPSS Statistics 20.0 for Windows).

Results

AST, fasting blood sugar, plasma BCAA and tyrosine levels in HCVTgM

The dietary intake and body weight did not differ significantly between the three groups of mice. BCAA administration for 6 months significantly reduced the serum

AST ($P < 0.05$) and fasting blood sugar (FBS) levels ($P < 0.05$) compared with HCV TgM fed the excess-iron diet with casein (casein/iron group) (Table 1). However, the FBS levels remained higher in the HCVTgM fed the excess-iron diet with BCAA (BCAA/iron group) compared with the HCV TgM fed a normal rodent diet (control group) ($P < 0.05$). The casein/iron group had significantly lower plasma BCAA and the ratio of BCAA relative to tyrosine (BTR) levels ($P < 0.05$) compared with the BCAA/iron and control groups (Table 1). The tyrosine levels were significantly higher in the casein/iron group than the control group ($P < 0.05$).

Hepatic iron contents and hepcidin-25 levels in HCVTgM

The hepatic iron contents of HCVTgM fed the excess-iron diet with casein were significantly higher than those of HCVTgM fed an excess-iron diet with BCAA or a control diet at 6 months after the treatment commenced (Fig. 1A). The hepcidin levels of HCVTgM fed the excess-iron diet with BCAA were significantly higher than those of HCVTgM fed the excess-iron diet with casein or the control diet (Fig. 1A). The serum hepcidin to ferritin ratio was lower in patients with HCV (25). The serum hepcidin-25 to hepatic iron ratio was significantly higher in HCVTgM fed the excess-iron diet with BCAA compared with those fed the excess-iron diet with casein or the control diet.

ROS generation

BCAA administration resulted in significantly lower dROM levels and an increased BAP to dROM ratio (BAP/dROM) compared with casein administration ($P < 0.05$; Fig. 1B). Hepatic ROS production, which was determined by dihydroethidium staining, was significantly higher in HCVTgM fed the excess-iron diet with casein compared with those fed the excess-iron diet with BCAA or the control diet (Fig. 1C). The BAP/dROM ratios were negatively correlated with hepatic ROS production in all mice ($r = 0.8985$; $n = 15$; $P < 0.01$; Fig. 1D).

Table 1. Effects of casein/iron and branched-chain amino acids (BCAA)/iron diets on the liver to body weight ratios and blood chemistry results in hepatitis C virus transgenic mice

	Control	Casein/iron	BCAA/iron
Mice (*N*)	6	7	5
Liver weight/ Body weight (%)	3.32 ± 0.30	3.50 ± 0.60	2.97 ± 0.28
AST (IU/L)	61 ± 23	92 ± 47	39 ± 7‡
ALT (IU/L)	14 ± 4	61 ± 60	16 ± 4
FBS (mg/dl)	115 ± 11	299 ± 49†	184 ± 47†‡
Insulin (ng/ml)	0.89 ± 0.36	1.19 ± 0.20	0.93 ± 0.39
Albumin (g/dl)	2.82 ± 0.04	2.77 ± 0.15	2.96 ± 0.15
BCAA (nmol/ml)	313 ± 22	275 ± 31†	318 ± 35‡
Tyrosine (nmol/ml)	63 ± 5	82 ± 11†	69 ± 11
BTR	5.01 ± 0.20	3.41 ± 0.40†	4.67 ± 0.40‡

*Results are mean ± SD.

†$P < 0.05$ vs. transgenic mice expressing hepatitis C virus polyprotein (HCVTgM) on control diet for 6 months.

‡$P < 0.05$ vs. HCVTgM on excess-iron diet with casein for 6 months.

ALT, alanine aminotransferase; AST, aspartate aminotransferase; FBS, fasting blood sugar.

Factors that affected hepcidin upregulation

HCV-induced ROS production downregulates hepcidin transcription by inhibiting the C/EBPα DNA-binding activity of CHOP (14). Thus, we examined CHOP expression and the hepcidin mRNA levels. Hepatic CHOP expression was significantly lower and hepatic hepcidin expression was significantly higher in HCVTgM fed the excess-iron diet with BCAA compared with the levels in HCVTgM fed the excess-iron diet plus casein (Fig. 2A,B). The IL-6-gp130/signal transducer and activator of transcription are involved in the regulation of hepcidin transcription (26). Another pathway that regulates hepcidin expression involves the TGF-β/bone morphogenetic protein superfamily (27, 28). Thus, we examined the STAT-IL6 and SMAD-BMP signalling pathways. There were no differences in the phosphate STAT3, IL6, phosphor- SMAD1/5/8 and BMP6 expression levels between the BCAA and casein groups (Fig. 2C). In addition, HCV-induced oxidative stress inhibited hepcidin expression through increased histone deacetylase (HDAC) activity in cell culture system (29). HDAC activity of HCV TgM fed the excess-iron diet with BCAA was significantly lower than those of HCVTgM fed the excess-iron diet with casein or the control diet (Fig. S2). These results suggested that BCAA induced the upregulation of hepatic hepcidin by enhancing the antioxidant potential.

Hepatic steatosis and CPT1 expression

HCVTgM fed the excess-iron diet developed severe steatosis, including the centrilobular microvesicular type (15, 17). Previous studies showed that the antioxidant drugs N-acetylcysteine (NAC) and Stronger Neo-Minophagen C (SNMC) reduce the hepatic triglyceride levels in a dose-dependent manner (30, 31). In the present study, BCAA administration tended to reduce the hepatic triglyceride levels ($P = 0.055$; Fig. 3A).

Thus, we examined the effects of BCAA on CPT1 and CPT2, which are proteins that regulate long-chain fatty acid oxidation in mitochondria, and SREBP1 expression, which is a transcription factor that activates genes required for lipogenesis. Our previous study indicated that decreased CPT1 and increased SREBP1 expression contribute to the development of hepatic steatosis in HCVTgM fed an excess-iron diet (30). In the present study, CPT1 expression increased significantly in HCVTgM fed the excess-iron diet with BCAA after 6 months ($P < 0.05$, Fig. 3C), whereas CPT2 expression

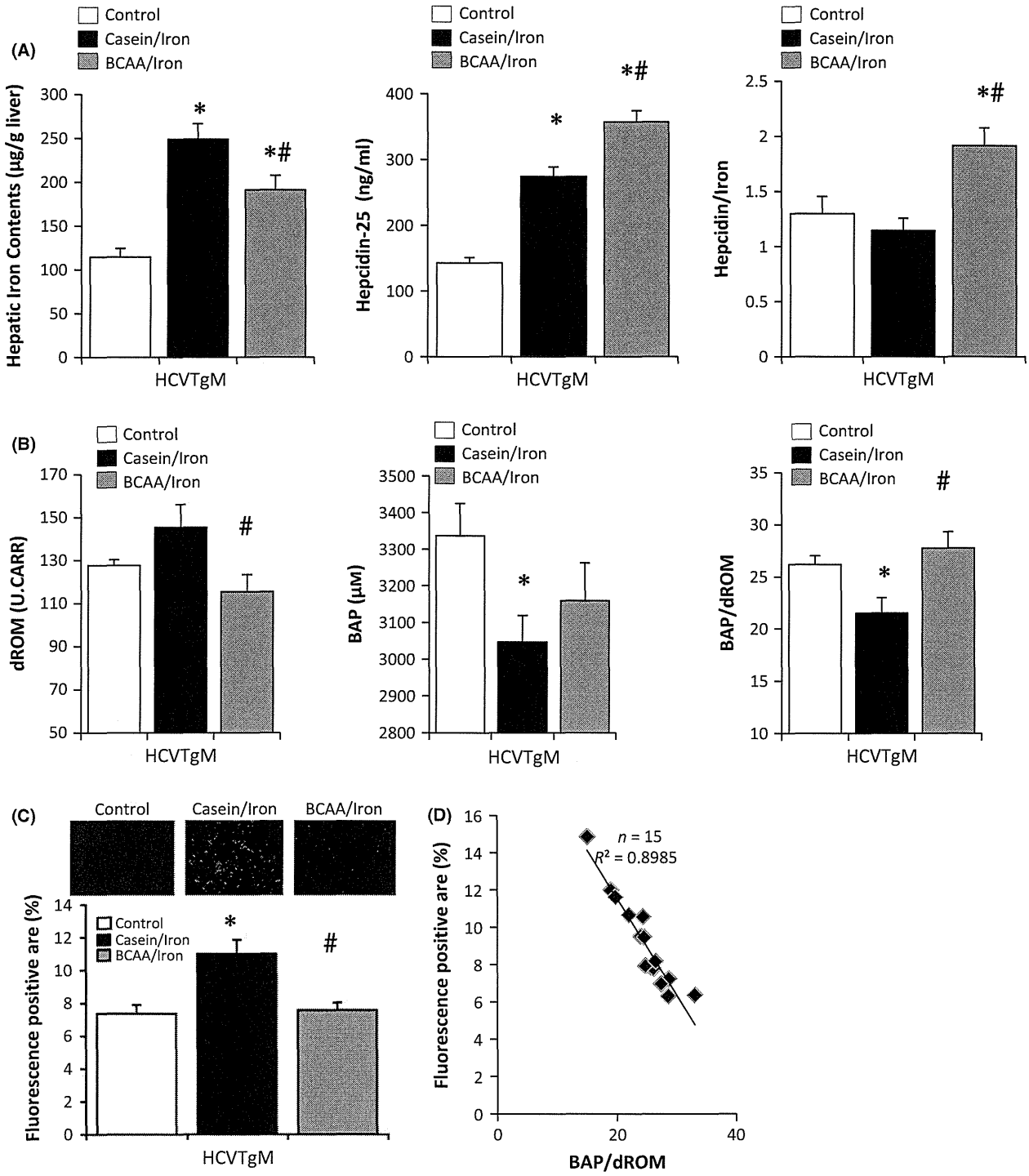

Fig. 1. (A) Hepatic iron contents, hepcidin-25 levels, and hepcidin-25 to iron content ratios (hepcidin/iron). (Left) Hepatic iron contents in mice at 6 months after starting treatment for the control (n = 6), casein/iron (n = 7) and BCAA/iron groups (n = 5). (Centre) Serum hepcidin-25 levels. (Right) The hepcidin/iron ratios were used as an index of the sensitivity of hepcidin upregulation against iron overload. (B) Oxidative stress markers in serum. (Left) dROM and (centre) BAP were measured at 6 months after starting treatment. (Right) The antioxidant status was determined as the BAP to dROM ratio. (C) Dihydroethidium fluorescence intensity was quantified for three randomly selected areas in digital images for the control (n = 3), casein/iron (n = 7), and BCAA/iron groups (n = 5) at 6 months after starting treatment. (D) Correlations between the BAP/dROM ratios and fluorescence-positive areas in liver. $^{*}P < 0.05$ vs control group; $^{\#}P < 0.05$ vs casein/iron group.

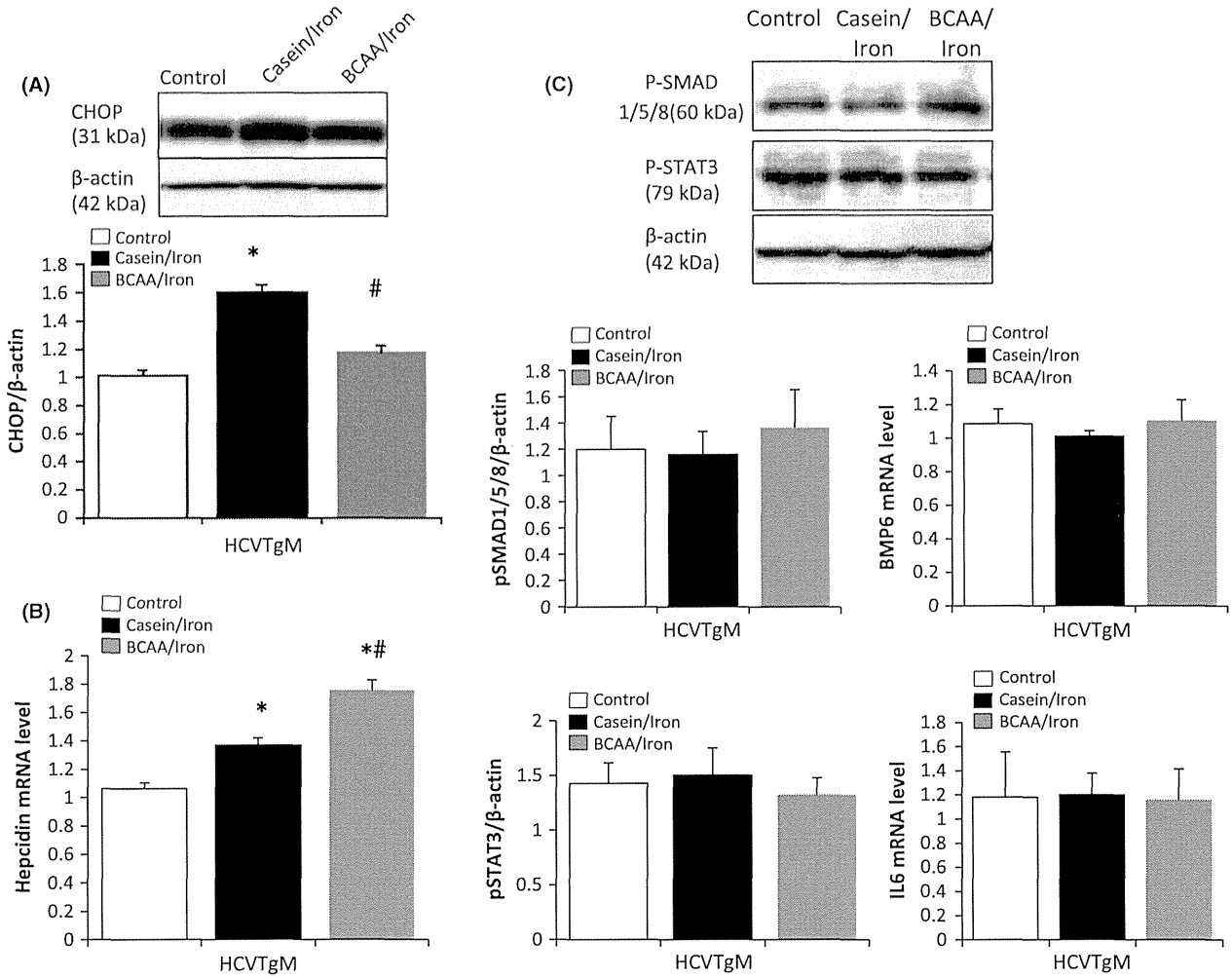

Fig. 2. (A) Immunoblots for CHOP after 6 months of treatment. (B) Liver hepcidin expression was determined for four mice in each group (C) Immunoblots for p-SMAD1/5/8 and (C) p-STAT3 after 6 months of treatment. (C) BMP6and (C) IL6 mRNA expression was determined for four mice in each group. The protein expression levels were normalized against that of β-actin. $^{*}P < 0.05$ vs control group; $^{\#}P < 0.05$ vs casein/iron group.

did not increase significantly. However, SREBP1 expression did not decrease in HCVTgM fed the excess-iron diet with BCAA ($P = 0.082$; Fig. 3B). These results suggest that the administration of BCAA was insufficient to prevent iron-induced steatosis in HCVTgM because BCAA failed to reduce SREBP1 expression.

SOD2 expression and mitochondrial complex I activity

CPT1 is localized to the mitochondrial outer membrane. Decreased CPT1 expression may be related to the HCV core protein's association with the mitochondrial outer membrane. The HCV core protein interacts with mitochondria complex I, which generates ROS (13). Alterations in the mitochondrial ultrastructure were observed in HCVTgM fed the excess-iron diet after 6 months, as described previously (15, 30). We examined whether BCAA supplementation reduced iron- and HCV-induced mitochondrial injury.

The mitochondrial SOD2 mRNA levels were significantly higher in HCVTgM fed the excess-iron diet with BCAA compared with those fed the excess-iron diet with casein or the control diet. The SOD2 expression levels in mice fed the excess-iron diet with casein were significantly lower than those fed the control diet. However, the SOD2 expression levels were restored by BCAA supplementation (Fig. 4A). After 6 months, the mitochondrial complex I expression levels were significantly lower in mice fed the excess-iron diet with casein compared with those fed the control diet. Similar to SOD2, the mitochondrial complex I expression levels were restored by BCAA supplementation (Fig. 4B).

The enzymatic activity of mitochondrial complex I was significantly lower in mice fed the excess-iron diet

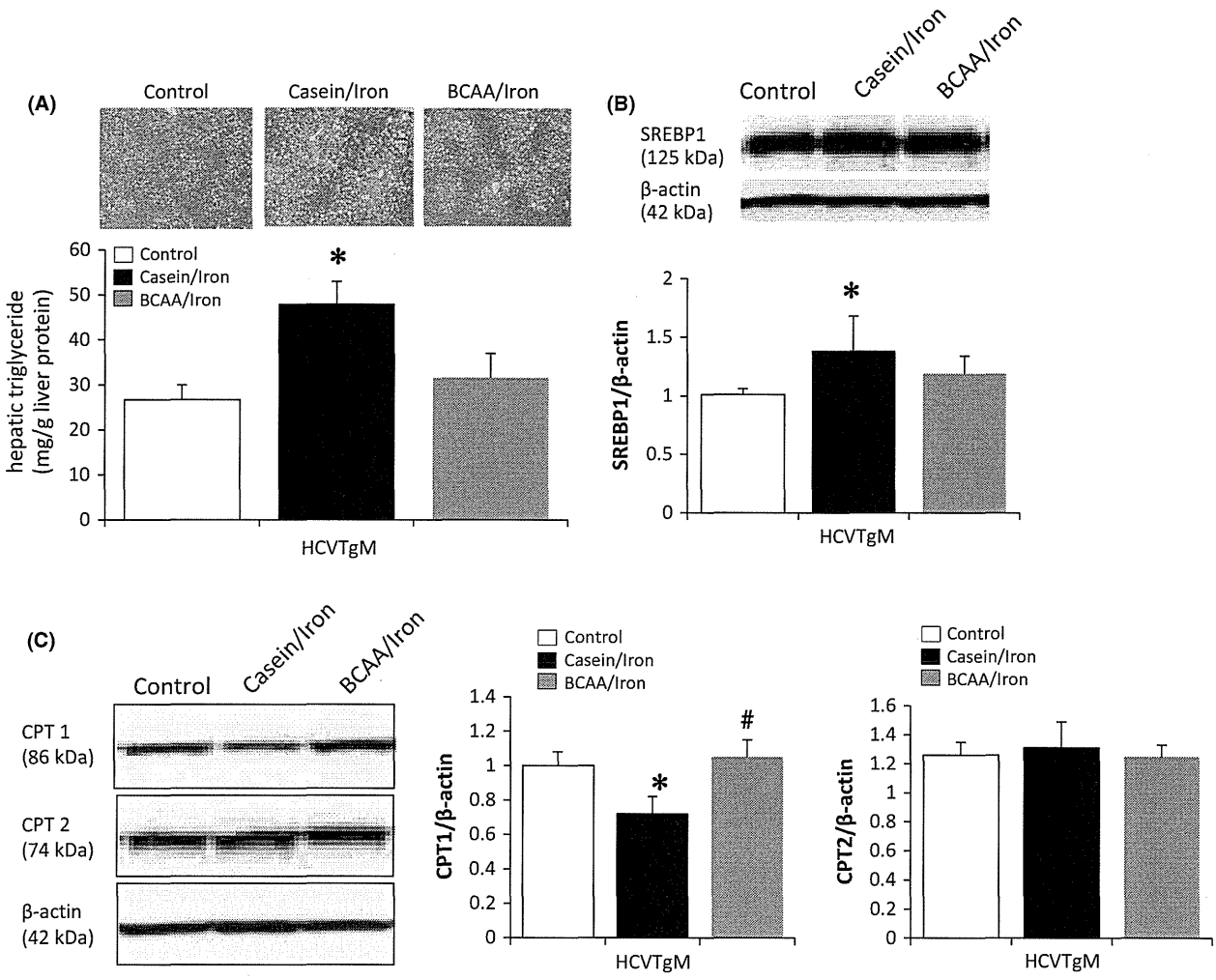

Fig. 3. (A) Hepatic steatosis in HCVTgM fed the excess-iron diet with BCAA and HCVTgM fed the excess-iron diet with casein after treatment for 6 months (haematoxylin and eosin, original magnification × 100). The hepatic triglyceride levels were determined. (B) Immunoblots of SREBP1, (C) CPT1, and (C) CPT2 in the livers of three mice from each group. $^{*}P < 0.05$ vs control group; $^{\#}P < 0.05$ vs casein/iron group.

with casein compared with those fed the control diet. The activity was restored by BCAA supplementation (Fig. 4C). Thus, these improvements in the mitochondrial complex I activity and CPT1, SOD2, and mitochondrial complex I expression indicate that BCAA may protect against the mitochondrial injury induced by HCV proteins and iron overload.

Antioxidant effects of BCAA supplementation in patients with HCV-related severe fibrosis

Next, we determined whether oral BCAA supplementation reduced oxidative stress and affected iron metabolism in patients with HCV-related advanced liver fibrosis. We assigned 25 patients to receive either BCAA supplementation (BCAA group; $n = 12$) or follow-up without treatment (non-BCAA group; $n = 13$). There were no differences in the clinical characteristics, oxidative stress markers, or iron metabolic markers at baseline between these groups (Table 2). Serum albumin and AST levels in BCAA group tended to be lower than those in non-BCAA group, although these differences were not statistically significant ($P = 0.071$ and $P = 0.074$ respectively).

The dROM levels increased significantly at weeks 24 and 48 in the non-BCAA group, whereas they did not in the BCAA group. The BAP levels also increased at weeks 12 and 24 in the non-BCAA group, and at weeks 12, 24 and 48 in the BCAA group (Table 3). The BAP/dROM ratio, an indicator of antioxidant potential, decreased significantly at week 48 in the non-BCAA group, but increased at weeks 24 and 48 in the BCAA group. This suggests that the BAP levels of the non-BCAA group increased in response to oxidative stress, while the increased BAP levels in the BCAA group indicated enhanced antioxidant potential.